Electronic Supplementary Information

X-shaped π-conjugated fluorophores enable cooperative ion-pair recognition with multicolour emission

Ryota Tazawa, Kaho Watanabe, Kei Mizuguchi, Shoki Mizoguchi, Takayuki Chiba, Shuji Okada, and Ryohei Yamakado*

Department of Organic Materials Science, Graduate School of Organic Materials Science, Yamagata University, Yonezawa 992–8510, Japan

Table of Contents

1. Synthetic procedures and spectroscopic data

General procedures.

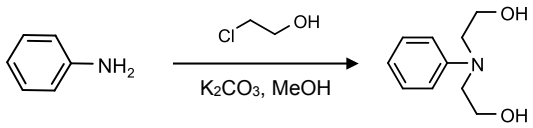

2-[(2-Hydroxyethyl)(phenyl)amino]ethan-1-ol[S1]

2-Chloroethanol (4.2 mL, 43.6 mmol) was added to a solution of aniline (1.0 mL, 10.9 mmol) and K_2CO_3 (4.45 g, 3.22 mmol) in MeOH (5 mL), and the mixture was stirred overnight at 40 °C. When the reaction was completed, the mixture was diluted with cold water (10 mL), and stirred for 5 minute. The mixture was extracted with CH_2Cl_2 and the organic layer was washed with cold water. A combined organic phase was dried over Na_2SO_4 and solvents were removed by a rotary evaporator. The residue was chromatographed over silica gel column (SiO_2; eluent: hexane/ EtOAc = 1/2) to afford 2-[(2-hydroxyethyl)(phenyl)amino]ethan-1-ol as a white solid (0.81 g, 4.46 mmol, 39%).

^{1}H-NMR (500 MHz, $CDCl_3$, δ) 7.23 (2H, dd, J = 8.6, 7.2 Hz), 6.74 (1H, t, J = 7.2 Hz), 6.69 (2H, d, J = 8.6 Hz), 3.85 (4H, t, J = 4.9 Hz), 3.58 (4H, t, J = 4.9 Hz), 3.41 (2H, s)

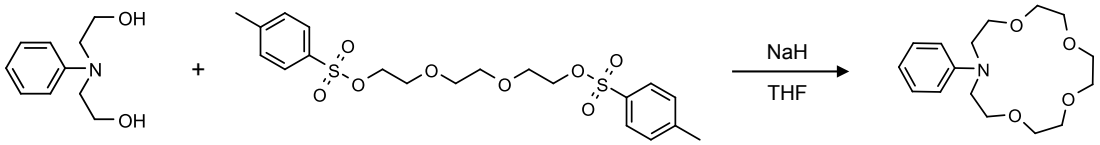

13-Phenyl-1,4,7,10-tetraoxa-13-azacyclopentadecane[S2]

NaH (1.54 g, 38.0 mmol) was added to a solution of 2-[(2-hydroxyethyl)(phenyl)amino]ethan-1-ol (5.50 g, 30.0 mmol) in dry THF (400 mL) and heated at reflux temperature. Then the solution of triethyleneglycolbis(*p*-toluenesulfonate) (4.30 g, 9.37 mmol) in dry THF (300 mL) was slowly added dropwise to the reaction mixture, and refluxing was continued for another 24 h. When the reaction was completed, the mixture cooled, then filtered and washed with THF. The solvents were removed by a rotary evaporator and the residue was chromatographed over silica gel column (SiO_2; eluent: EtOAc/ CH_2Cl_2 = 1:9, R_f = 0.3) to afford 13-phenyl-1,4,7,10-tetraoxa-13-azacyclopentadecane as a white liquid (1.68 g, 5.70 mmol, 61%).

^{1}H-NMR (400 MHz, $CDCl_3$, δ) 7.21 (2H, t, J = 7.8 Hz), 6.66 (3H, t, J = 4.3 Hz,), 3.76 (4H, t, J = 6.2 Hz), 3.66 (12H, m), 3.60 (4H, t, J = 6.2 Hz)

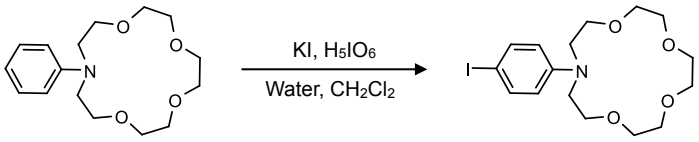

13-(4-Iodophenyl)-1,4,7,10-tetraoxa-13-azacyclopentadecane[S2]

13-Phenyl-1,4,7,10-tetraoxa-13-azacyclopentadecane (0.260 g, 0.880 mmol) in CH_2Cl_2 (3 mL) were added to KI (0.175 g, 1.05 mmol) and H_5IO_6 (0.134 g, 0.588 mmol) in H_2O (3 mL). The mixture was stirred vigorously for 2 h at r.t. When the reaction was completed, the mixture was washed with aq. $Na_2S_2O_3$ (10%). The aqueous fraction was extracted with CH_2Cl_2. The organic layer was dried over Na_2SO_4, and the solvent was removed by a rotary evaporator. The residue was chromatographed over silica gel column (SiO_2; eluent: $CHCl_3$/MeOH = 10:1, R_f = 0.5) to afford 13-(4-iodophenyl)-1,4,7,10-tetraoxa-13-azacyclopentadecane as a brown liquid (0.321 g, 0.761 mmol, 87%).

^{1}H-NMR (500 MHz, $CDCl_3$, δ) 7.43 (2H, dd, J = 6.9, 2.3 Hz), 6.44 (2H, dd, J = 6.9, 2.3 Hz), 3.72 (4H, t, J = 6.0 Hz), 3.68–3.63 (12H, m), 3.55 (4H, t, J = 6.0 Hz)

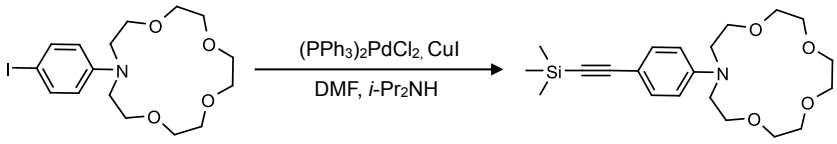

13-{4-[2-(Trimethylsilyl)ethynyl]phenyl}-1,4,7,10-tetraoxa-13-azacyclopentadecane[S2]

A mixture of 13-(4-iodophenyl)-1,4,7,10-tetraoxa-13-azacyclopentadecane (220 mg, 0.522 mmol), trimethylsilylacetylene (0.37 mL, 2.61 mmol), $Pd(PPh_3)_2Cl_2$ (37.0 mg, 0.0527 mmol), and CuI (10 mg, 0.0522 mmol) in 5 mL of *i*-Pr_2NH and 15 mL of dry DMF was stirred in an atmosphere of N_2 at 70 °C for 24 h. When the reaction was

completed, the reaction mixture was cooled at r.t., and the solvent was removed by rotary evaporator. The residue was chromatographed over silica gel column (SiO_2; eluent: EtOAc, R_f = 0.5) to afford 13-{4-[2-(trimethylsilyl)ethynyl]phenyl}-1,4,7,10-tetraoxa-13-azacyclopentadecane as a brown liquid (0.183 g, 0.467 mmol, 90%).
^{1}H-NMR (400 MHz, $CDCl_3$, δ) 7.30 (2H, d, J = 9.0 Hz), 6.55 (2H, d, J = 9.0 Hz), 3.74 (4H, t, J = 6.2 Hz), 3.66 (12H, m), 3.59 (4H, t, J = 6.2 Hz), 0.23 (9H, s)

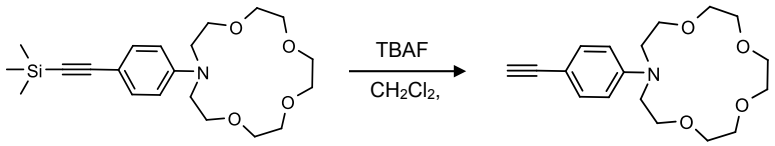

13-(4-Ethynylphenyl)-1,4,7,10-tetraoxa-13-azacyclopentadecane[S2]

TBAF (395 mg, 1.25 mmol) in CH_2Cl_2 (10 mL) was added to a solution of 13-{4-[2-(trimethylsilyl)ethynyl]phenyl}-1,4,7,10-tetraoxa-13-azacyclopentadecane (170 mg, 0.434 mmol) in CH_2Cl_2 (50 mL), and the mixture was stirred for 4 h at 0 °C. After dichloromethane was added, the reaction mixture was washed with water. A combined organic phase was dried over Na_2SO_4, and solvents were removed by a rotary evaporator. The residue was chromatographed over silica gel column (SiO_2; eluent: EtOAc, R_f = 0.5) to afford 13-(4-ethynylphenyl)-1,4,7,10-tetraoxa-13-azacyclopentadecane as a brown liquid (0.136 g, 0.425 mmol, 98%).
^{1}H-NMR (600 MHz, $CDCl_3$, δ) 7.33 (2H, d, J = 9.0 Hz), 6.58 (2H, d, J = 9.0 Hz), 3.74 (4H, t, J = 6.2 Hz), 3.68–3.63 (12H, m), 3.60 (4H, t, J = 6.2 Hz), 2.97 (1H, s)

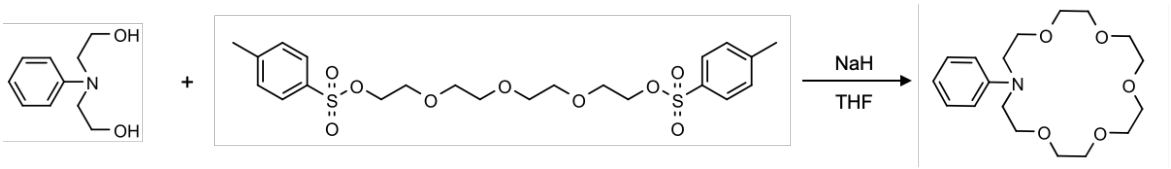

16-Phenyl-1,4,7,10,13-pentaoxa-16-azacyclooctadecane[S2]

NaH (781 mg, 19.6 mmol) was added to a solution of 2-[(2-hydroxyethyl)(phenyl)amino]ethan-1-ol (1.5 g, 8.28 mmol) in dry THF (300 mL) and heated at reflux temperature. Then the solution of tetraethyleneglycolbis(*p*-toluenesulfonate) (1.52 g, 3.31 mmol) in dry THF (80 mL) was slowly added dropwise to the reaction mixture, and refluxing was continued for another 24 h. When the reaction was completed, the mixture cooled, then filtered and washed with THF. The solvents were removed by a rotary evaporator and the residue was chromatographed over silica gel column (SiO_2; eluent: EtOAc/MeOH = 10:1, R_f = 0.2) to afford 16-phenyl-1,4,7,10,13-pentaoxa-16-azacyclooctadecane as a white liquid (0.598 g, 1.76 mmol, 21%).
^{1}H-NMR (500 MHz, $CDCl_3$, δ) 7.22–7.17 (2H, dd, J = 8.8, 7.3 Hz), 6.68 (2H, d J =8.8 Hz), 6.65 (1H, d, J = 7.3 Hz), 3.71–3.61 (24H, m)

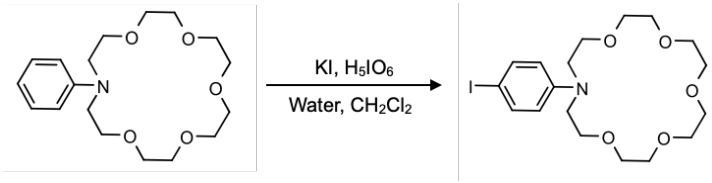

16-(4-Iodophenyl)-1,4,7,10,13-pentaoxa-16-azacyclooctadecane[S2]

16-Phenyl-1,4,7,10,13-pentaoxa-16-azacyclooctadecane (0.498 g, 1.47 mmol) in CH_2Cl_2 (6 mL) were added KI (0.293 g, 1.77 mmol) and H_5IO_6 (0.402 g, 1.77 mmol) in H_2O (5 mL). The mixture was stirred vigorously for 2 h at r.t. When the reaction was completed, the mixture was washed with aq. $Na_2S_2O_3$ (10 wt%). The aqueous fraction was extracted with CH_2Cl_2. The organic layer was dried over Na_2SO_4, and the solvent was removed by a rotary evaporator. The residue was chromatographed over silica gel column (SiO_2; eluent: EtOAc, R_f = 0.3) to afford 16-(4-iodophenyl)-1,4,7,10,13-pentaoxa-16-azacyclooctadecane as a brown liquid (0.484 g, 1.04 mmol, 71%).
^{1}H-NMR (500 MHz, $CDCl_3$, δ) 7.42 (2H, dd, J = 6.9, 2.3 Hz), 6.47 (2H, dd, J = 6.9, 2.3Hz), 3.68–3.56 (24H, m)

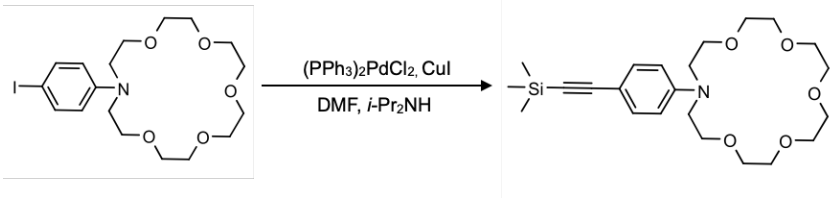

16-{4-[2-(Trimethylsilyl)ethynyl]phenyl}-1,4,7,10,13-pentaoxa-16-azacyclooctadecane[S1]

A mixture of 16-(4-iodophenyl)-1,4,7,10,13-pentaoxa-16-azacyclooctadecane (0.300 g, 0.644 mmol), trimethylsilylacetylene (0.37 mL, 2.61 mmol), $Pd(PPh_3)_2Cl_2$ (45.2 mg, 0.0644 mol), and CuI (12.3 mg, 0.0644 mmol) in 7 mL of *i*-Pr_2NH and 20 mL of dry DMF was stirred in an atmosphere of N_2 at 70 °C for 24 h. When the reaction was completed, the reaction mixture was cooled at r.t., and the solvent was removed by rotary evaporator. The residue was chromatographed over silica gel column (SiO_2; eluent: EtOAc, R_f = 0.3) to afford 16-{4-[2-(trimethylsilyl)ethynyl]phenyl}-1,4,7,10,13-pentaoxa-16-azacyclooctadecane as a brown liquid (0.265 g, 0.608 mmol, 94%).

^{1}H-NMR (500 MHz, $CDCl_3$, δ) 7.30 (2H, dd, *J* = 6.9, 2.3 Hz), 6.57 (2H, dd, *J* = 6.9, 2.3 Hz), 3.69–3.61 (24H, m), 0.22 (9H, s)

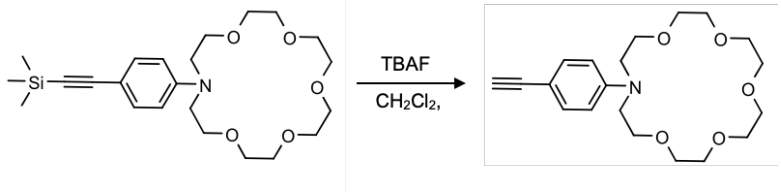

16-(4-Ethynylphenyl)-1,4,7,10,13-pentaoxa-16-azacyclooctadecane[S2]

TBAF (0.520 g, 1.99 mmol) in CH_2Cl_2 (10 mL) was added to a solution of 16-{4-[2-(trimethylsilyl)ethynyl]phenyl}-1,4,7,10,13-pentaoxa-16-azacyclooctadecane (0.260 g, 0.596 mmol) in CH_2Cl_2 (50 mL), and the mixture was stirred for 4 h at 0 °C. After dichloromethane was added, the reaction mixture was washed with water. A combined organic phase was dried over Na_2SO_4, and solvents were removed by a rotary evaporator. The residue was chromatographed over silica gel column (SiO_2; eluent: EtOAc, R_f = 0.3) to afford 16-(4-ethynylphenyl)-1,4,7,10,13-pentaoxa-16-azacyclooctadecane as a brown liquid (0.209 g, 0576 mmol, 97%).

^{1}H-NMR (500 MHz, $CDCl_3$, δ) 7.33 (2H, d, *J* =8.9 Hz), 6.60 (2H, d, *J* = 8.9 Hz), 3.70–3.62 (24H, m), 2.97 (1H, s)

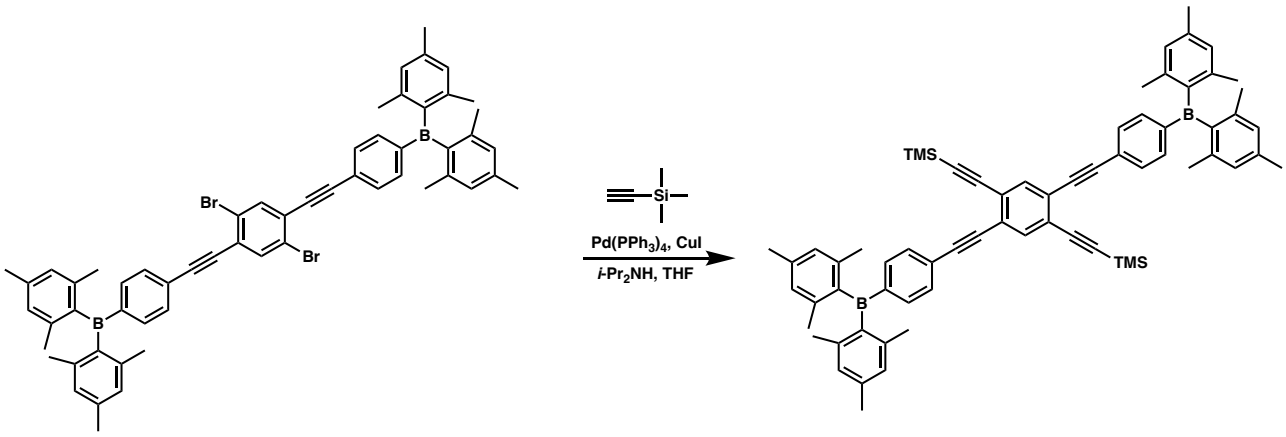

1,4-Bis[(trimethylsilyl)ethynyl]-2,5-bis{[(4-dimesitylboryl)phenyl]ethynyl}benzene

A mixture of 1,4-dibromo-2,5-bis{[(4-dimesitylboryl)phenyl]ethynyl}benzene[S3] (0.360 g, 0.386 mmol), trimethylsilylacetylene (0.10 mL, 0.723 mmol), $Pd(PPh_3)_4$ (108 mg, 0.0935 mol), and CuI (28 mg, 0.147 mmol) in 10 mL of *i*-Pr_2NH and 10 mL of dry THF was stirred in an atmosphere of N_2 at 70 °C for 24 h. When the reaction was completed, the reaction mixture was cooled at r.t., and the solvent was removed by rotary evaporator. The residue was chromatographed over a silica gel column (SiO_2; eluent: CH_2Cl_2/hexane = 1/6) to afford 1,4-Bis[(trimethylsilyl)ethynyl]-2,5-bis{[(4-dimesitylboryl)phenyl]ethynyl}benzene (178 mg, 0.184 mmol, 51 %) as a yellow solid.

^{1}H NMR (400 Hz, $CDCl_3$) δ (ppm): 7.68 (2H, s), 7.51 (8H, s), 6.84 (8H, s), 2.33 (12H, s), 2.01 (24H, s), 0.25 (18H, s)

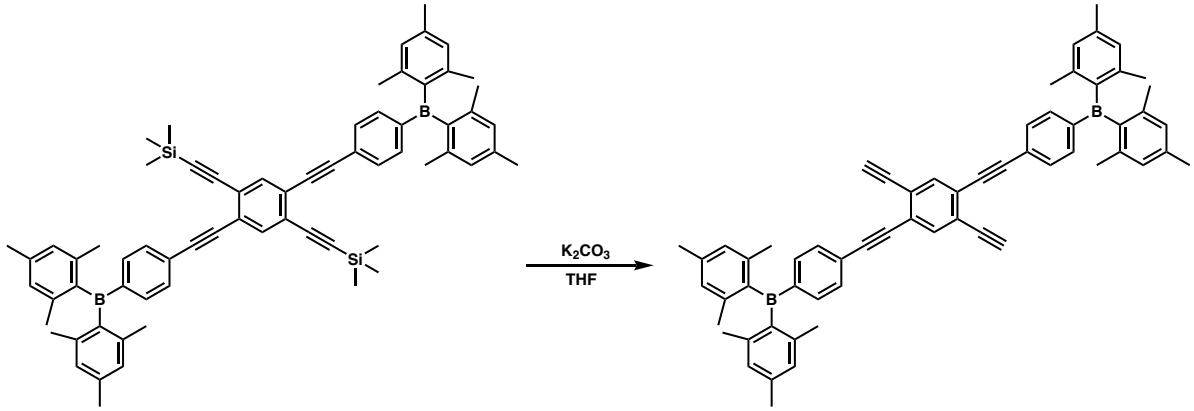

1,4-Diethynyl-2,5-bis{[(4-dimesitylboryl)phenyl]ethynyl}benzene

A mixture of 1,4-bis[(trimethylsilyl)ethynyl]-2,5-bis{[(4-dimesitylboryl)phenyl]ethynyl}benzene (0.176 g, 0.182 mmol) and K_2CO_3 (812 mg, 5.87 mmol) in THF (2 mL) and MeOH (4 mL) was stirred at room temperature for 24 h. After dichloromethane was added, the reaction mixture was washed with NH_4Cl aq. A combined organic phase was dried over Na_2SO_4, with the solvent removed by a rotary evaporator. The residue was chromatographed over silica gel column (SiO_2; eluent: CH_2Cl_2/hexane = 1/3, R_f = 0.4) to afford 1,4-diethynyl-2,5-bis{[(4-dimesitylboryl)phenyl]ethynyl}benzene as a brown solid (0.140 g, 0.177 mmol, 97%).

^{1}H NMR (400 Hz, $CDCl_3$) δ (ppm): 7.70 (2H, s), 7.51 (8H, s), 6.83 (8H, s), 3.45 (2H, s), 2.31 (12H, s), 2.00 (24H, s)

[S1] Bhange, D. S.; Sonawane, R. B.; Rasal, N. K.; Jagtap, S. V. *ChemistrySelect* **2020**, *5* (33), 10387–10390.
[S2] Paul, I.; Mittal, N.; De, S.; Bolte, M.; Schmittel, M. *J. Am. Chem. Soc.* **2019**, *141* (13), 5139–5143.
[S3] Morii, K.; Nabeta, H.; Yanbe, T.; Watanabe, K.; Sumikoshi, S.; Chiba, T.; Yamakado, R.; Okada, S. *ChemistrySelect* **2024**, *9* (1), e202305008.

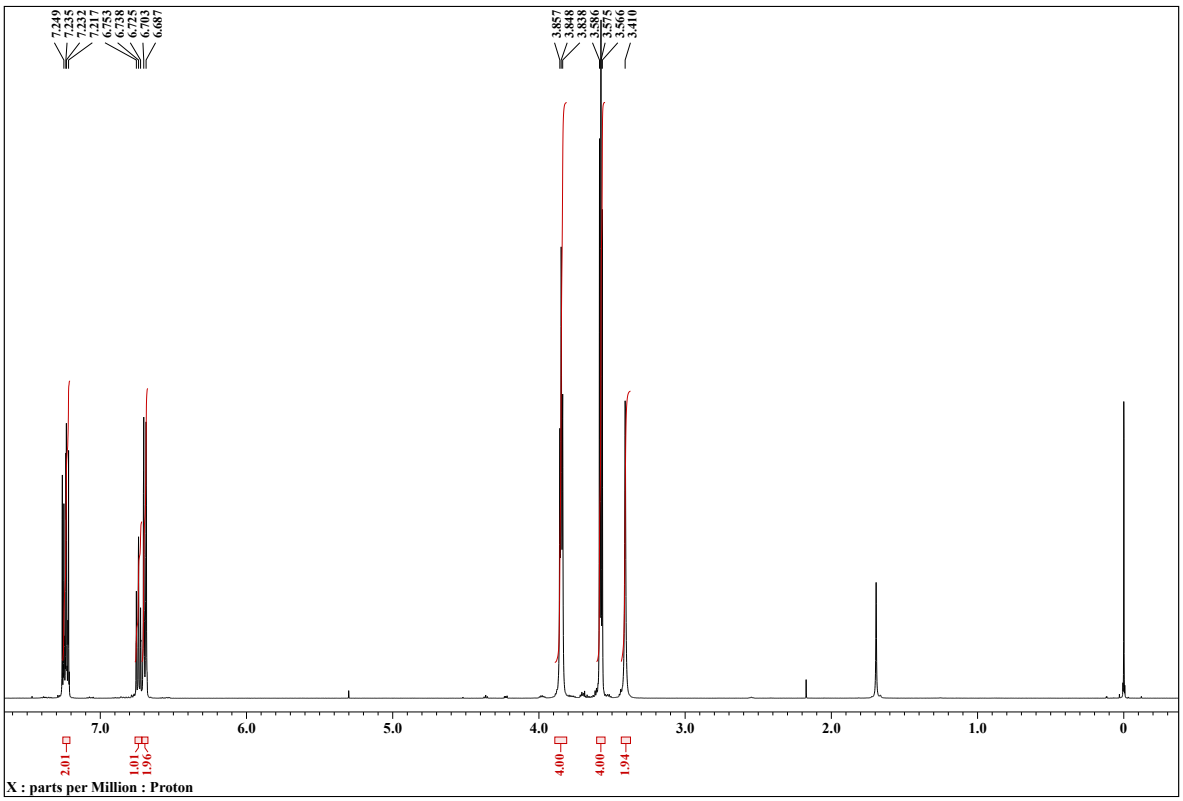

Fig. S1 [1]H-NMR spectrum of 2-[(2-hydroxyethyl)(phenyl)amino]ethan-1-ol in $CDCl_3$.

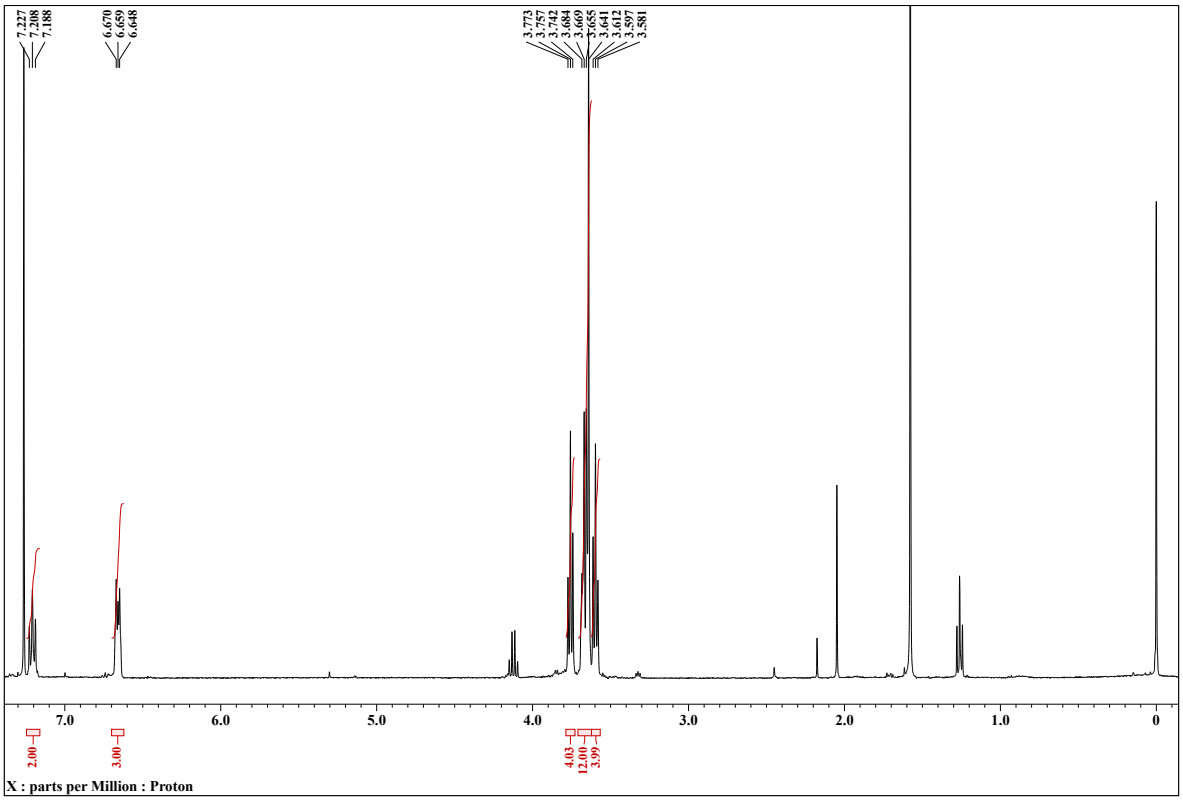

Fig. S2 [1]H-NMR spectrum of 13-phenyl-1,4,7,10-tetraoxa-13-azacyclopentadecane in $CDCl_3$.

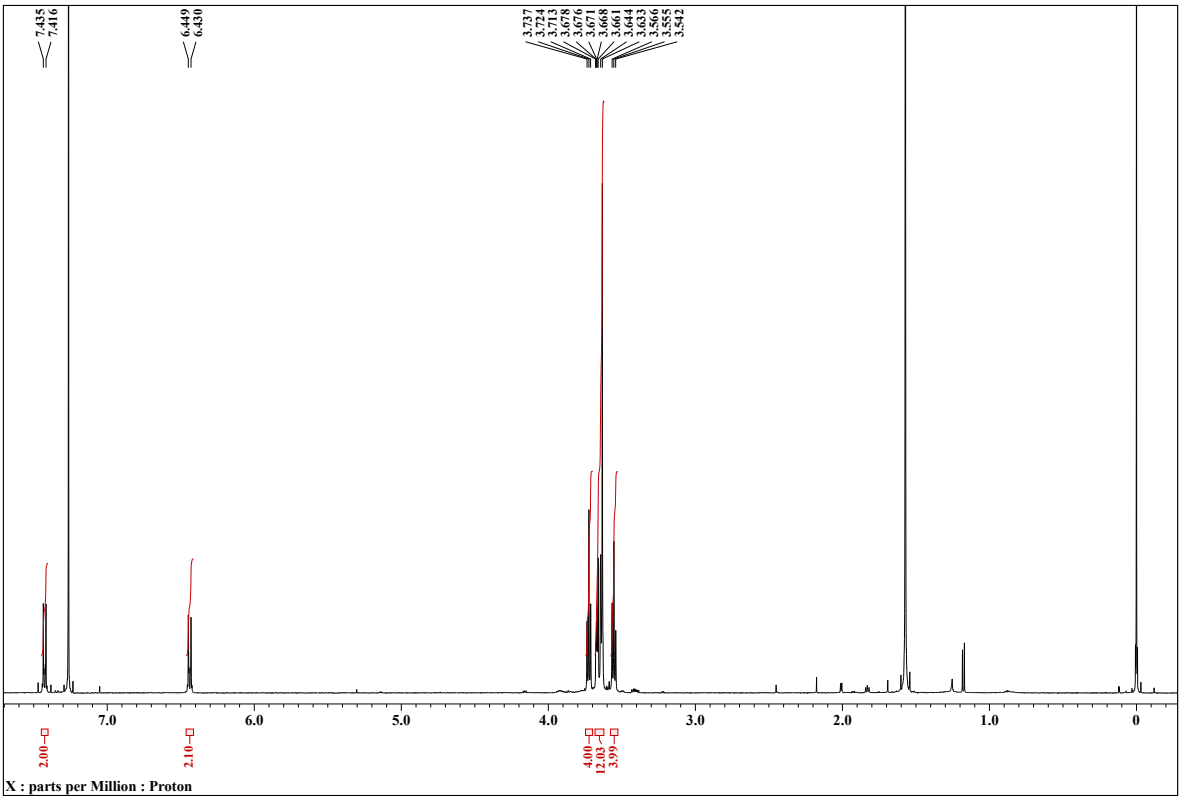

Fig. S3 [1]H-NMR spectrum of 13-(4-iodophenyl)-1,4,7,10-tetraoxa-13-azacyclopentadecane in $CDCl_3$.

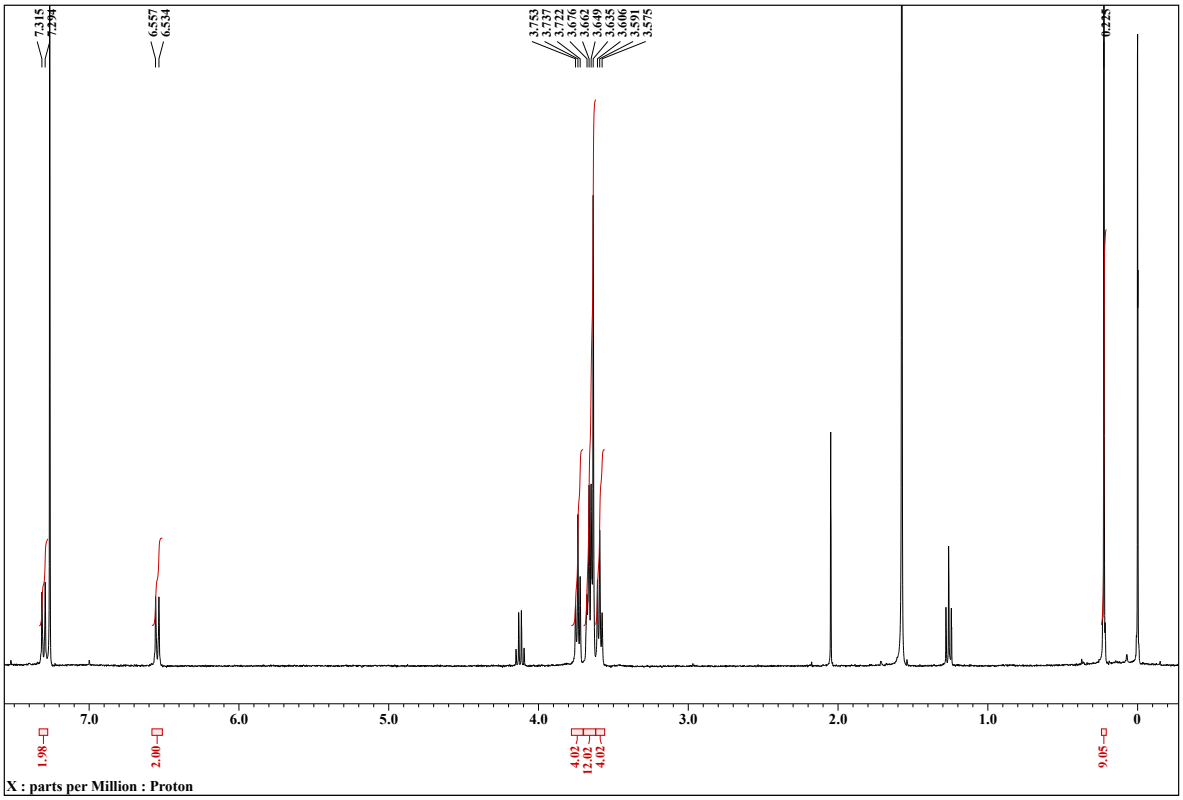

Fig. S4 [1]H-NMR spectrum of 13-{4-[2-(trimethylsilyl)ethynyl]phenyl}-1,4,7,10-tetraoxa-13-azacyclopentadecane in $CDCl_3$.

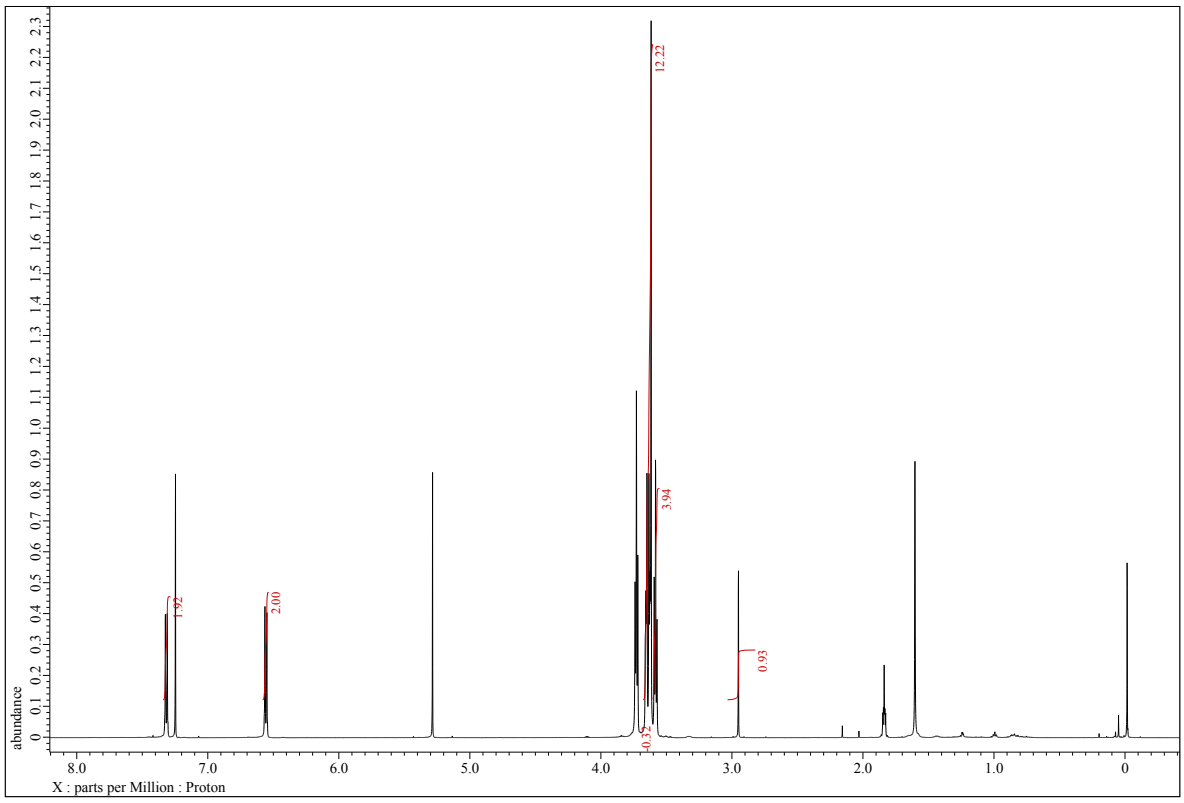

Fig. S5 ^{1}H-NMR spectrum of 13-(4-ethynylphenyl)-1,4,7,10-tetraoxa-13-azacyclopentadecane in $CDCl_3$.

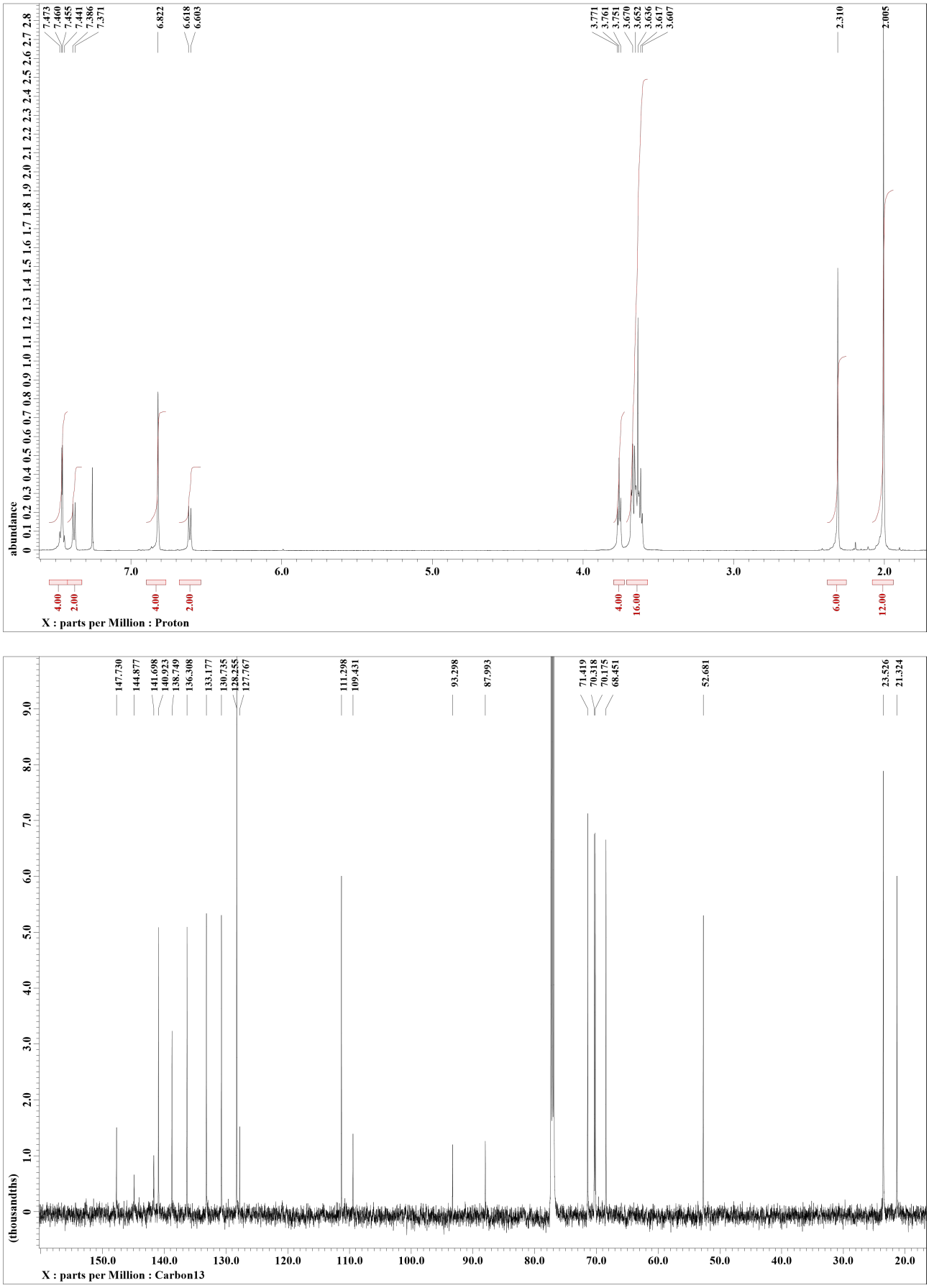

Fig. S6 ^{1}H (top) and ^{13}C (bottom) NMR spectra of **L1** in $CDCl_3$.

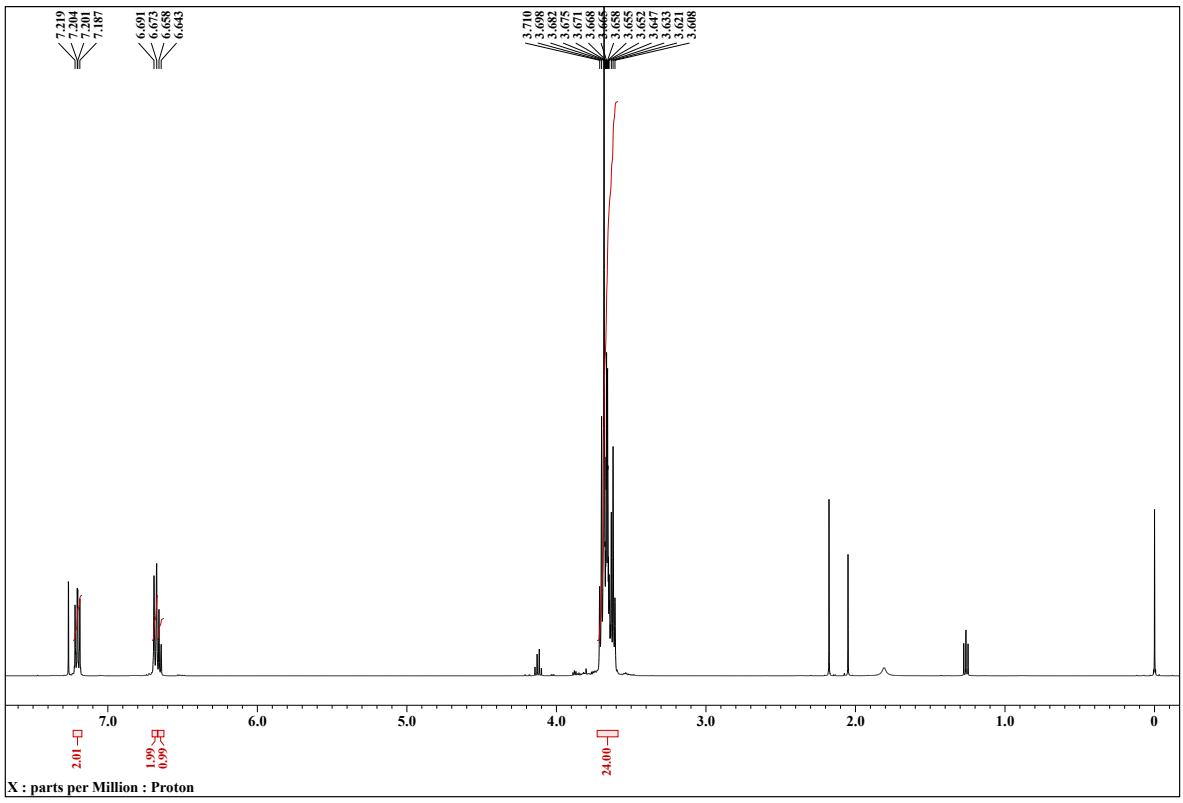

Fig. S7 [1]H-NMR spectrum of 16-phenyl-1,4,7,10,13-pentaoxa-16-azacyclooctadecane in $CDCl_3$.

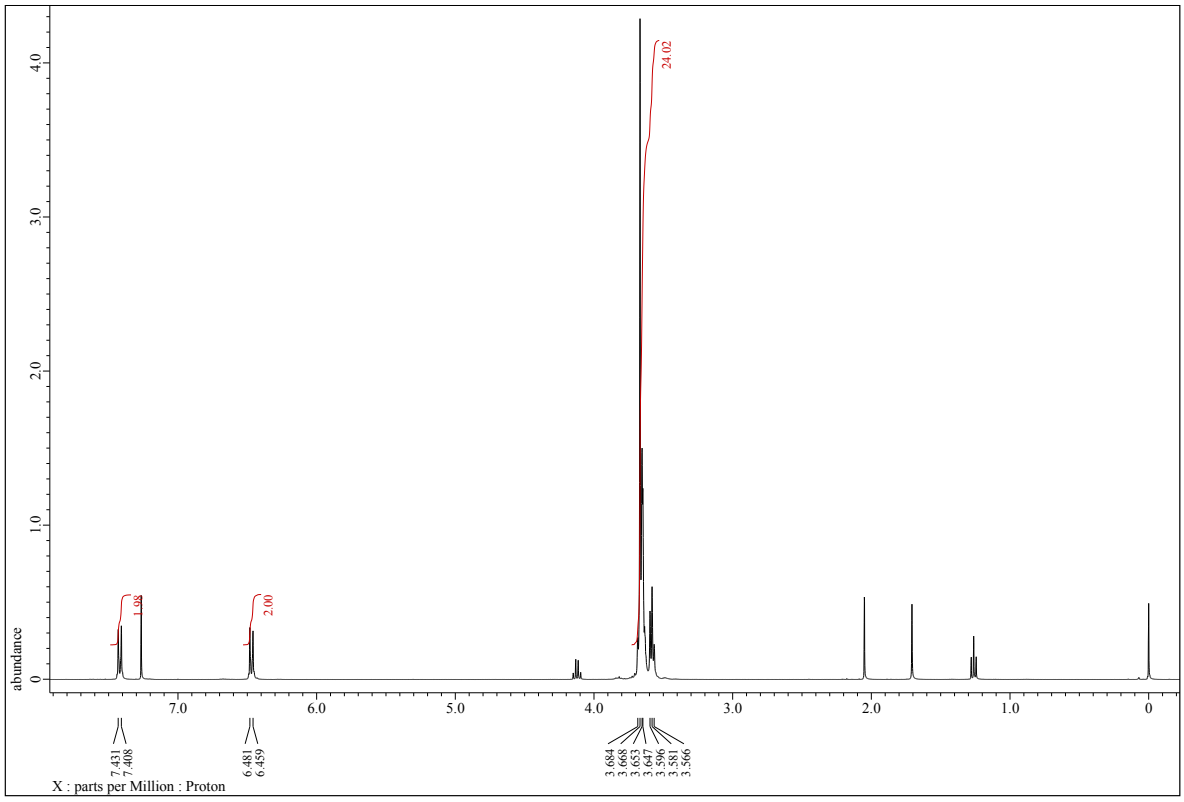

Fig. S8 [1]H-NMR spectrum of 16-(4-iodophenyl)-1,4,7,10,13-pentaoxa-16-azacyclooctadecane in $CDCl_3$.

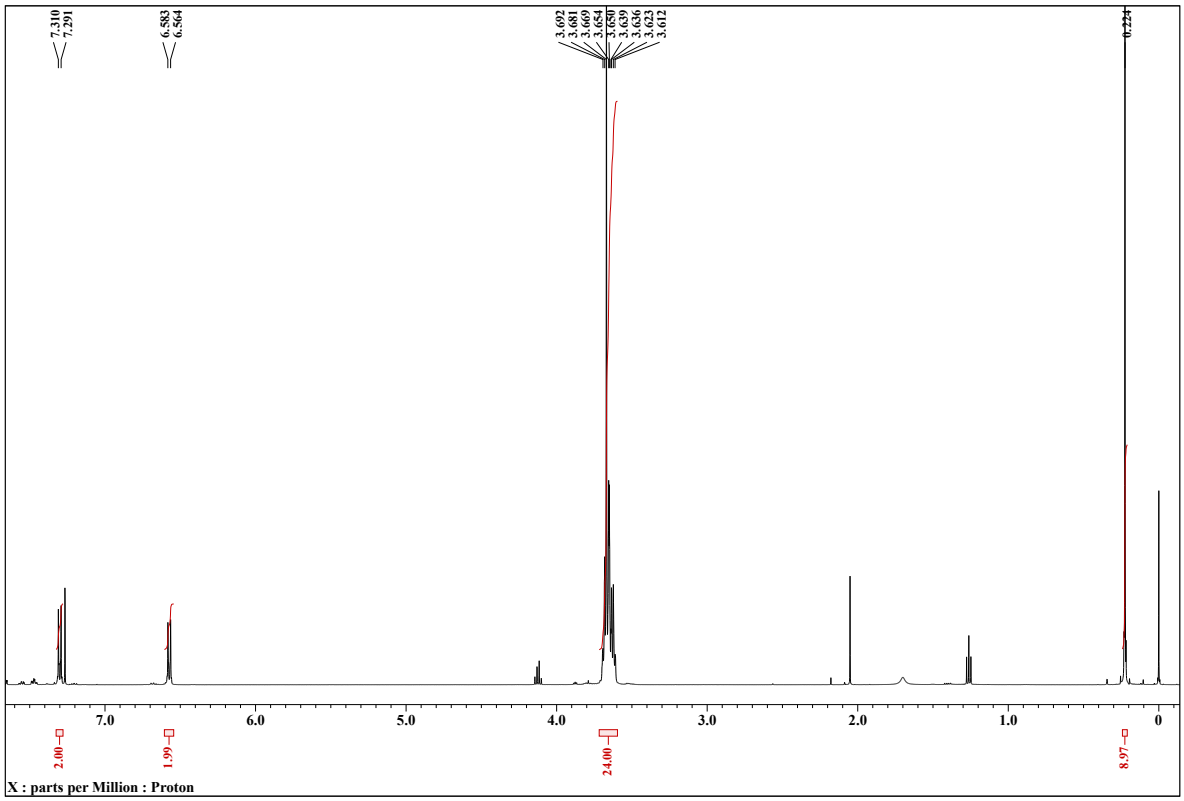

Fig. S9 ^{1}H-NMR spectrum of 16-{4-[2-(trimethylsilyl)ethynyl]phenyl}-1,4,7,10,13-pentaoxa-16-azacyclooctadecane in $CDCl_3$.

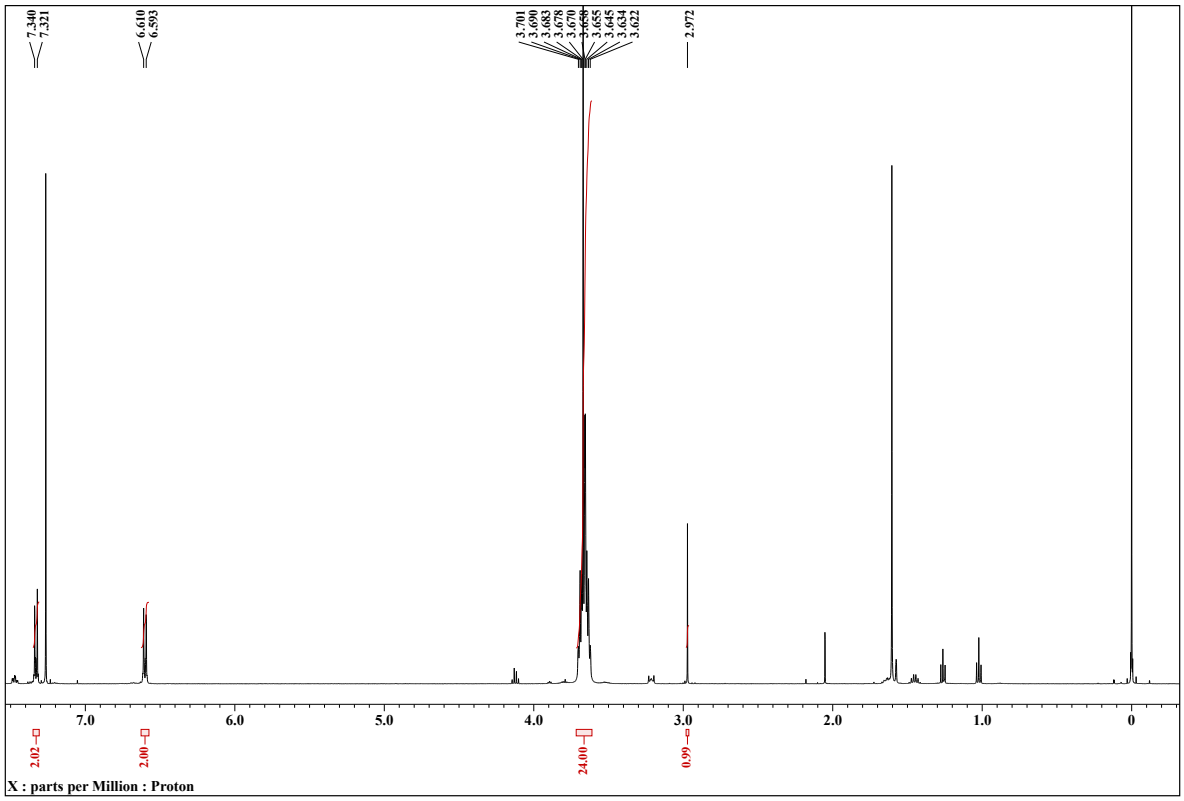

Fig. S10 ^{1}H-NMR spectrum of 16-(4-ethynylphenyl)-1,4,7,10,13-pentaoxa-16-azacyclooctadecane in $CDCl_3$.

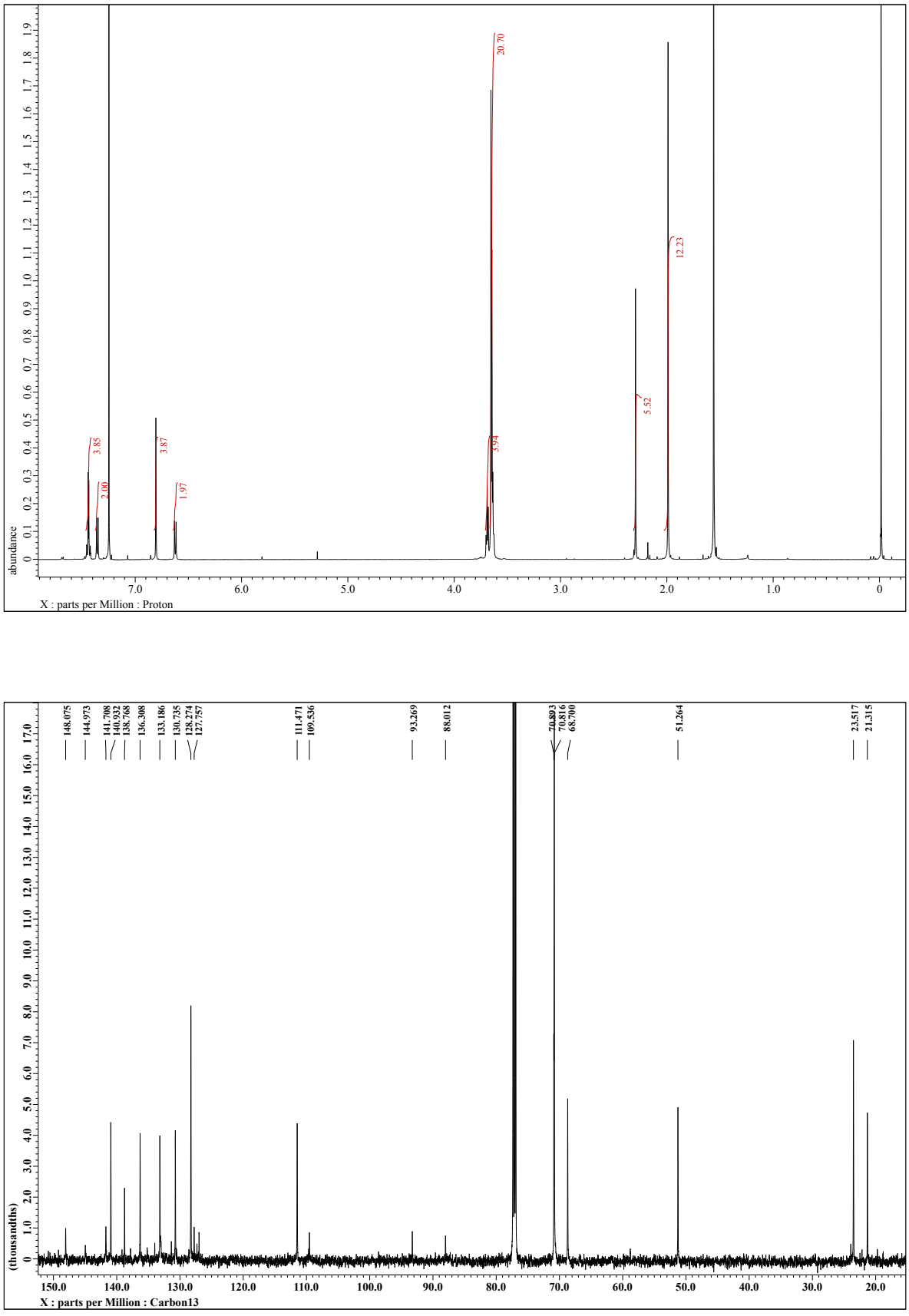

Fig. S11 ^{1}H (top) and ^{13}C (bottom) NMR spectra of **L2** in $CDCl_3$.

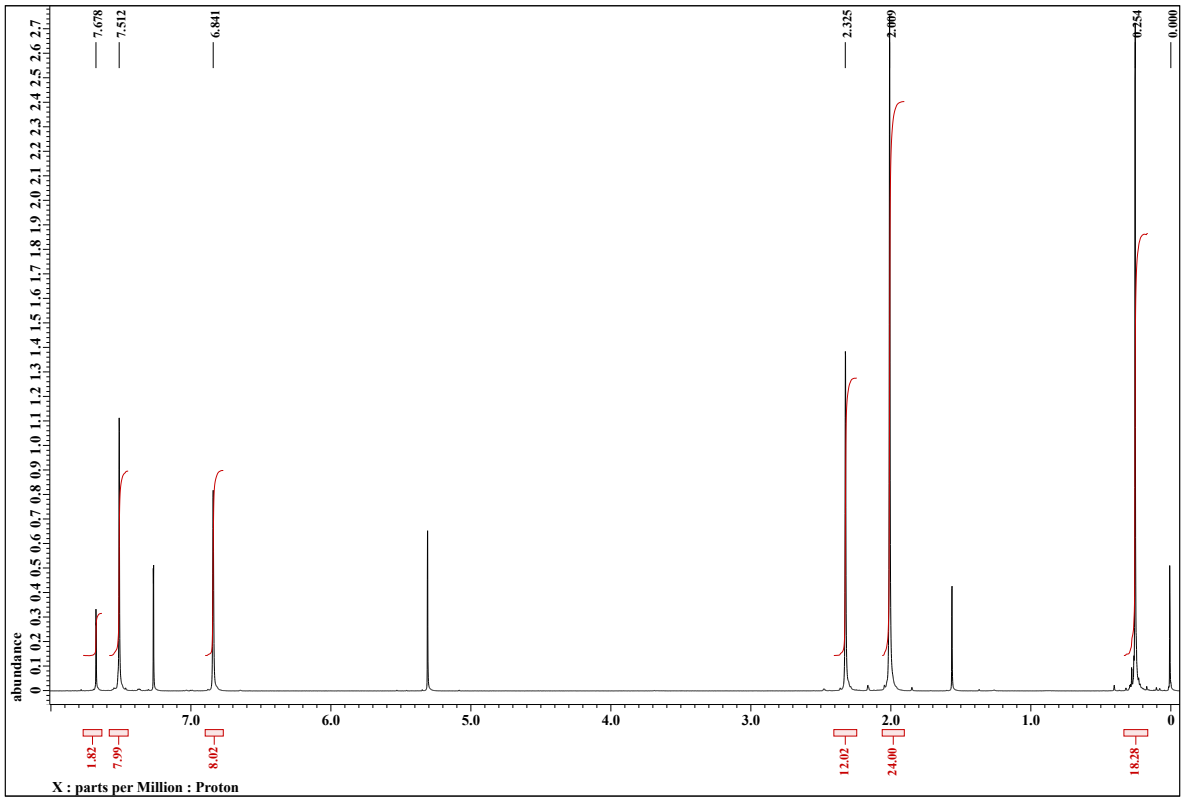

Fig. S12 ^{1}H NMR spectrum of 1,4-bis[(trimethylsilyl)ethynyl]-2,5-bis{[(4-dimesitylboryl)phenyl]ethynyl}benzene in $CDCl_3$.

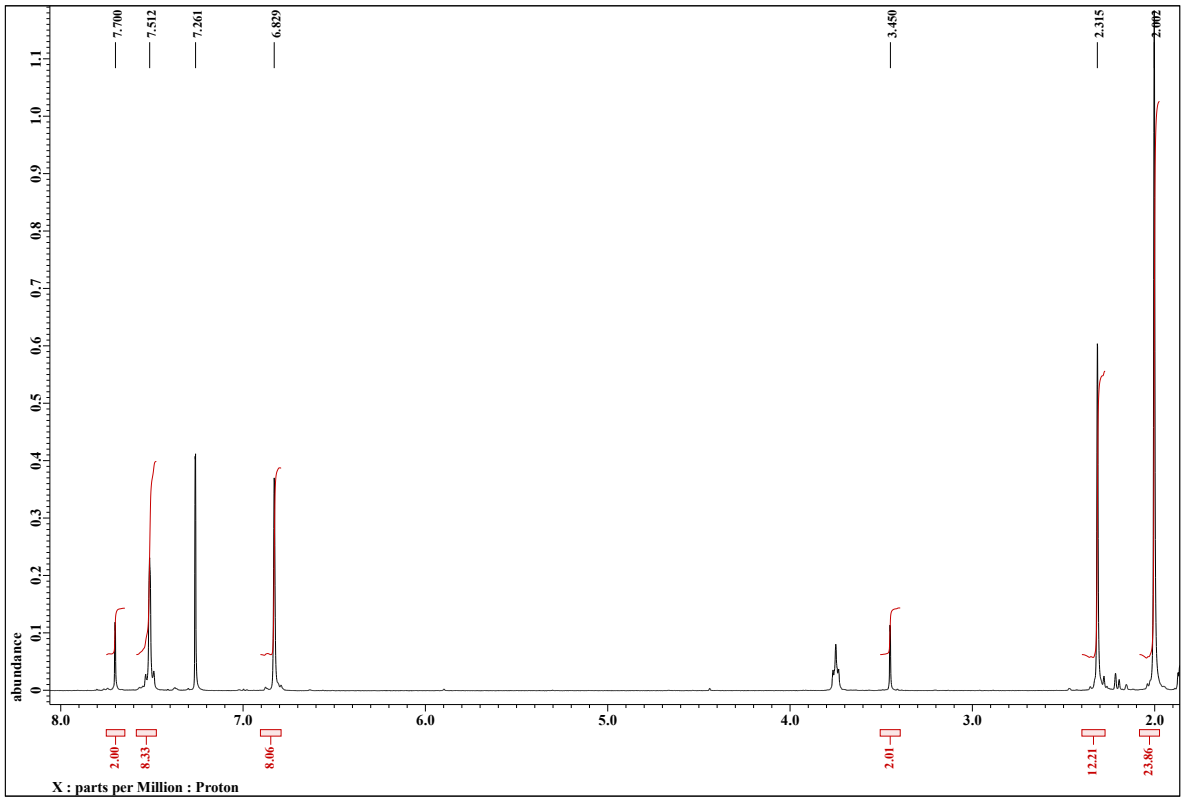

Fig. S13 ^{1}H NMR spectrum of 1,4-diethynyl-2,5-bis{[(4-dimesitylboryl)phenyl]ethynyl}benzene in $CDCl_3$.

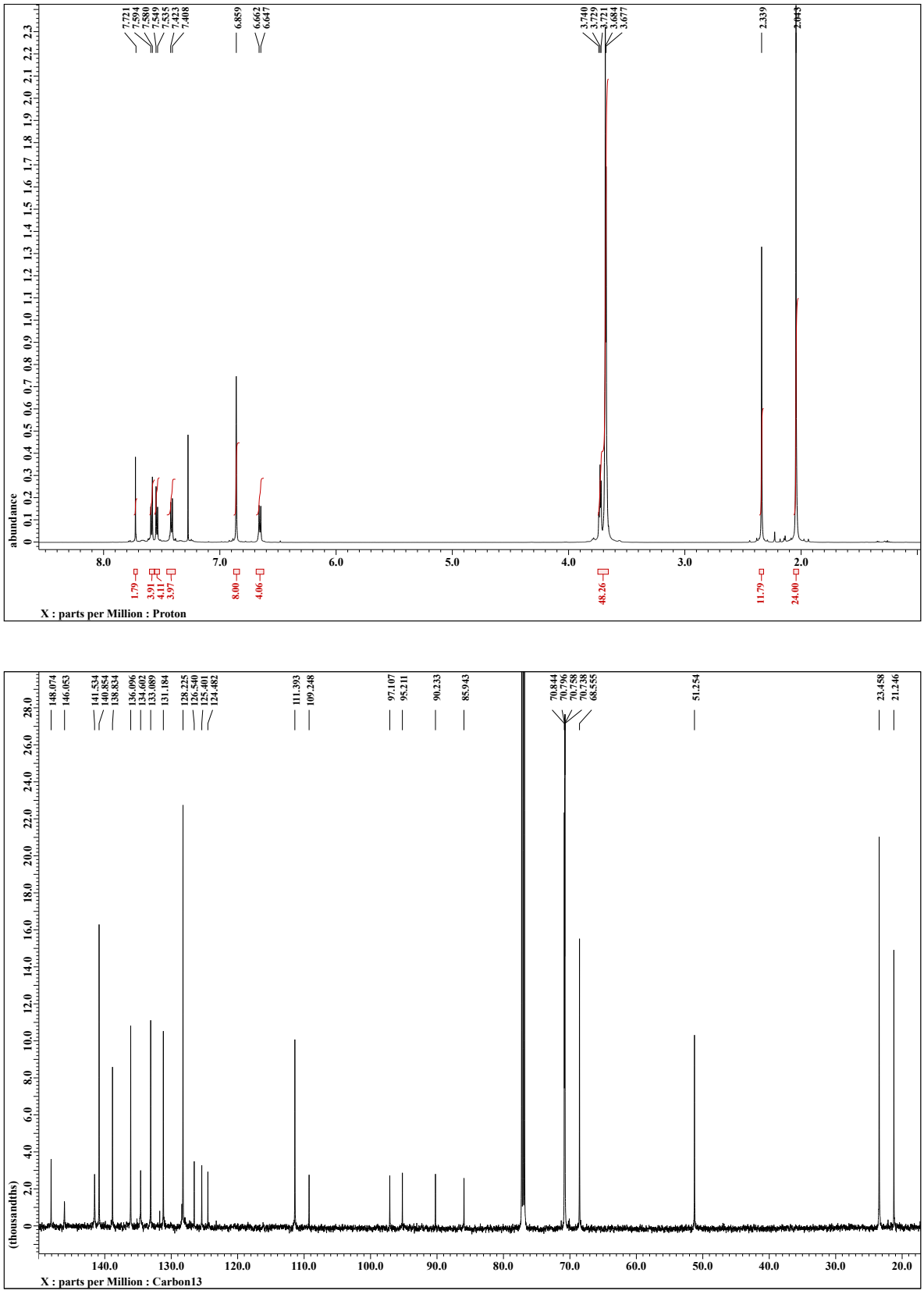

Fig. S14 ^{1}H (top) and ^{13}C (bottom) NMR spectra of **X1** in $CDCl_3$.

2. Optical properties

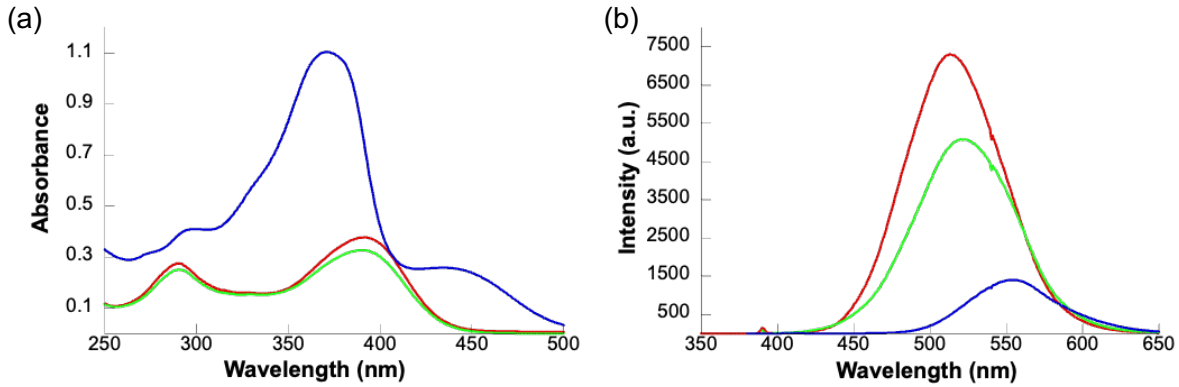

Fig. S15 (a) UV/vis absorption and (b) fluorescence spectra of **L1** (red), **L2** (green), and **X1** (blue) in CH_2Cl_2 (10^{-5} M).

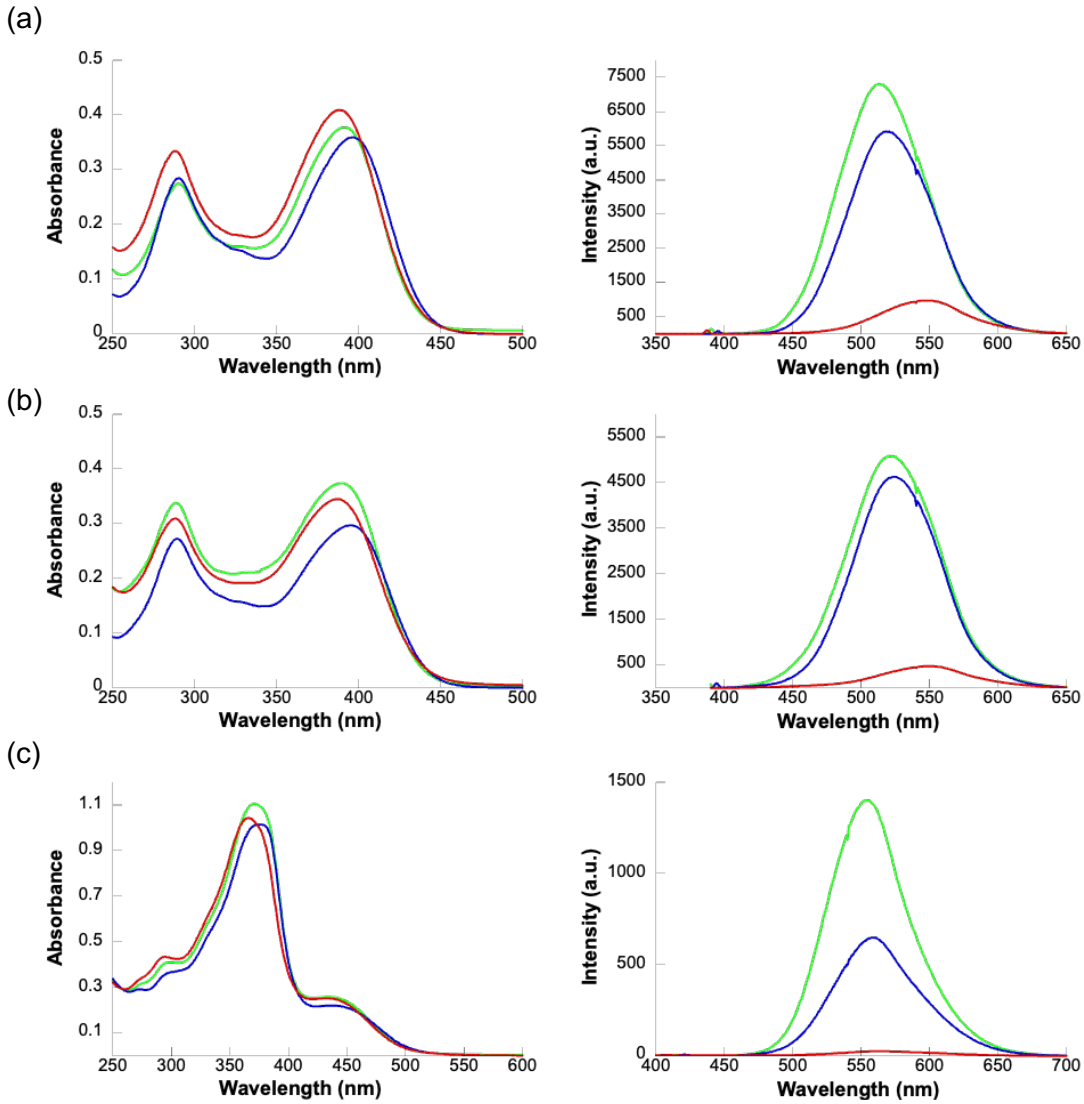

Fig. S16 UV/vis absorption (left) and fluorescence spectra (right) of (a) **L1**, (b) **L2**, and (c) **X1** in CH_2Cl_2 (green), THF (blue), and MeCN (red) (10^{-5} M).

3. Ion-binding properties

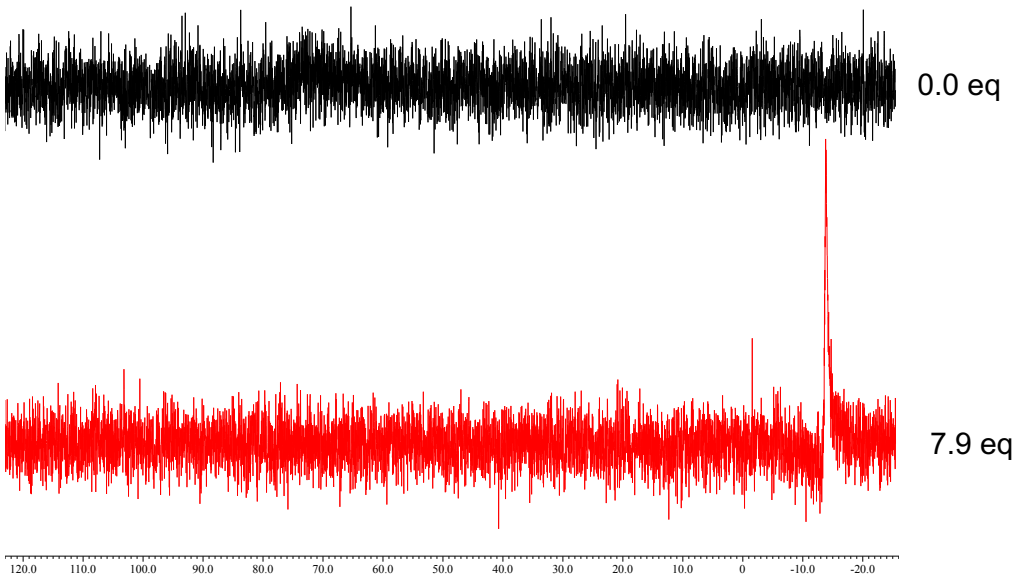

Fig. S17 ^{11}B NMR spectral changes of **L1** (1.2 mM) upon the addition of CN^- as TBA salt in CD_2Cl_2/CD_3CN (1:1) at 25 °C. The ^{11}B NMR spectrum of **L1** showed broad signal at approximately 75 ppm, consistent with the trigonal planar geometry of the boron centre. Upon the addition of CN^- as a tetrabutylammonium (TBA^+) salt, the original signal intensities decreased, and new peak appeared at –13.8 ppm.

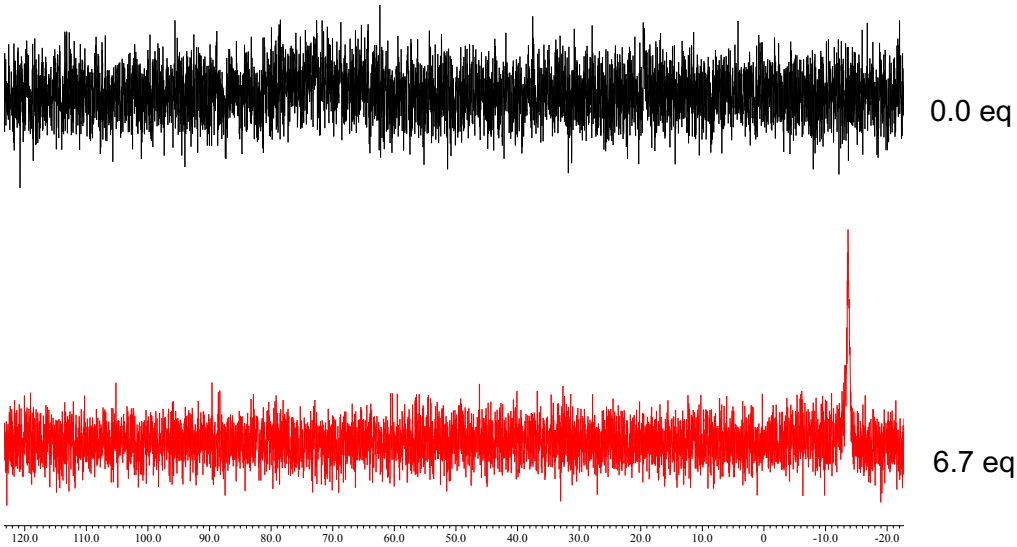

Fig. S18 ^{11}B NMR spectral changes of **L2** (1.2 mM) upon the addition of CN^- as TBA salt in CD_2Cl_2/CD_3CN (1:1) at 25 °C. ^{11}B NMR spectrum of **L2** showed broad signal at approximately 75 ppm, consistent with the trigonal planar geometry of the boron centre. Upon the addition of CN^- as TBA^+ salt, the original signal intensities decreased, and new peak appeared at –13.6 ppm.

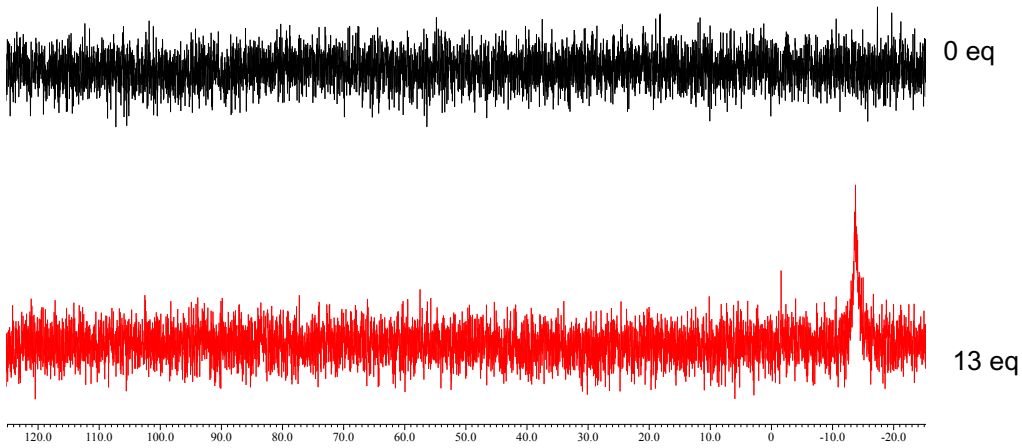

Fig. S19 ^{11}B NMR spectral changes of **X1** (1.2 mM) upon the addition of CN^- as TBA salt in CD_2Cl_2/CD_3CN (1:1) at 25 °C. ^{11}B NMR spectrum of **X1** showed broad signal at approximately 75 ppm, consistent with the trigonal planar geometry of the boron centre. Upon the addition of CN^- as TBA^+ salt, the original signal intensities decreased, and new peak appeared at –14.3 ppm.

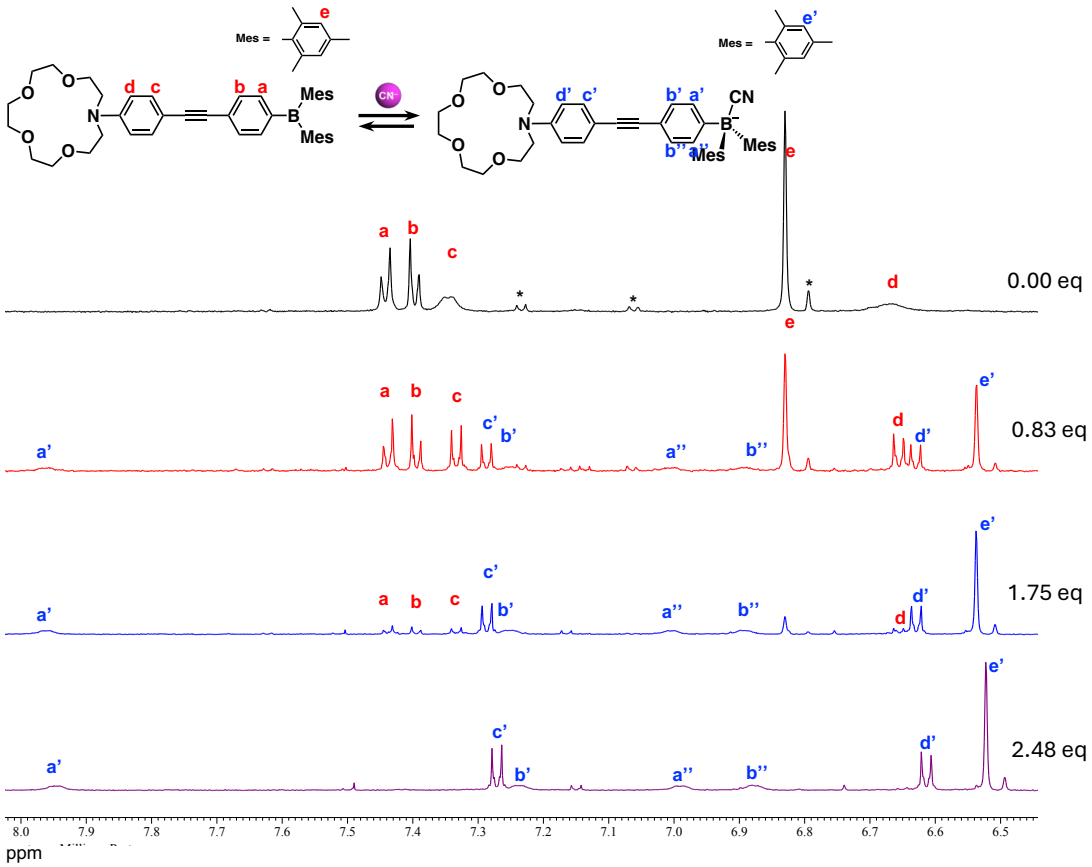

Fig. S20 ^{1}H NMR spectral changes of **L1** (1.2 mM) upon the addition of CN^- as TBA^+ salt in CD_2Cl_2/CD_3CN (1:1) at 25 °C. The protons of the boron-substituted phenyl group split into four distinct signals (a', a'', b', and b'') upon anion association. This splitting arises from steric hindrance that restricts rotation about the B–C bond, thereby lowering the molecular symmetry. Notably, the proton (a') subjected to the deshielding effect of the CN^- exhibited a pronounced downfield shift. These observations are in good agreement with the NMR spectra simulated by theoretical calculations. * was not observed when only dichloromethane was used, and was therefore presumed to originate from the formation of a complex with acetonitrile.

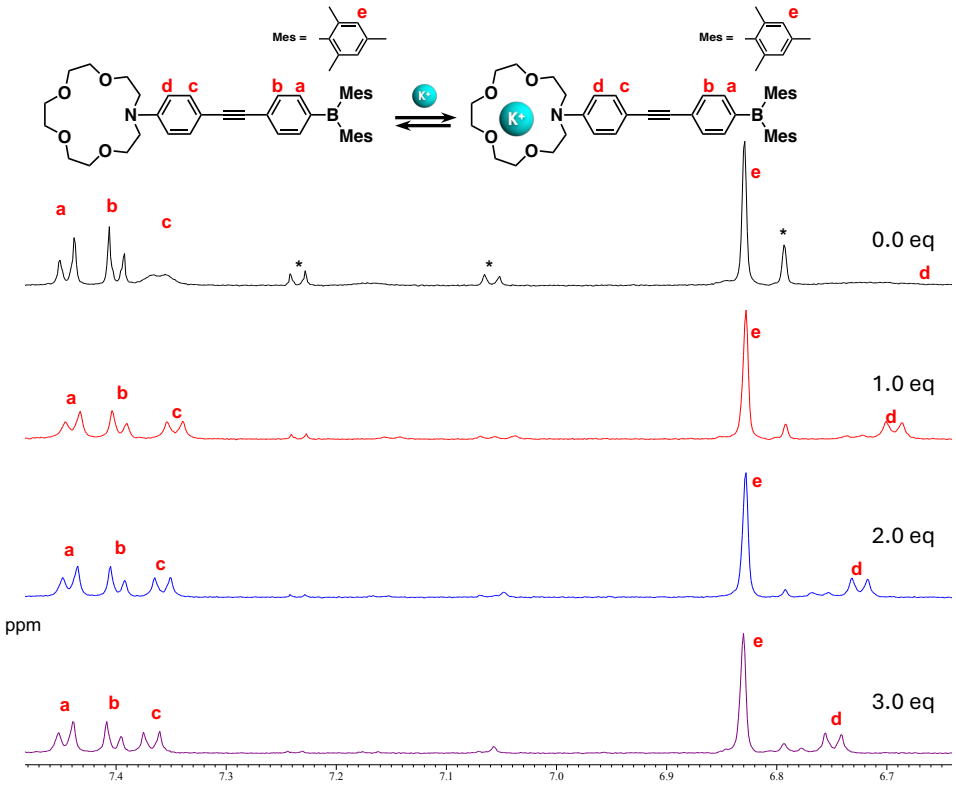

Fig. S21 ^{1}H NMR spectral changes of **L1** (1.2 mM) upon the addition of K^+ as PF_6^- salt in CD_2Cl_2/CD_3CN (1:1) at 25°C. * was not observed when only dichloromethane was used, and was therefore presumed to originate from the formation of a complex with acetonitrile.

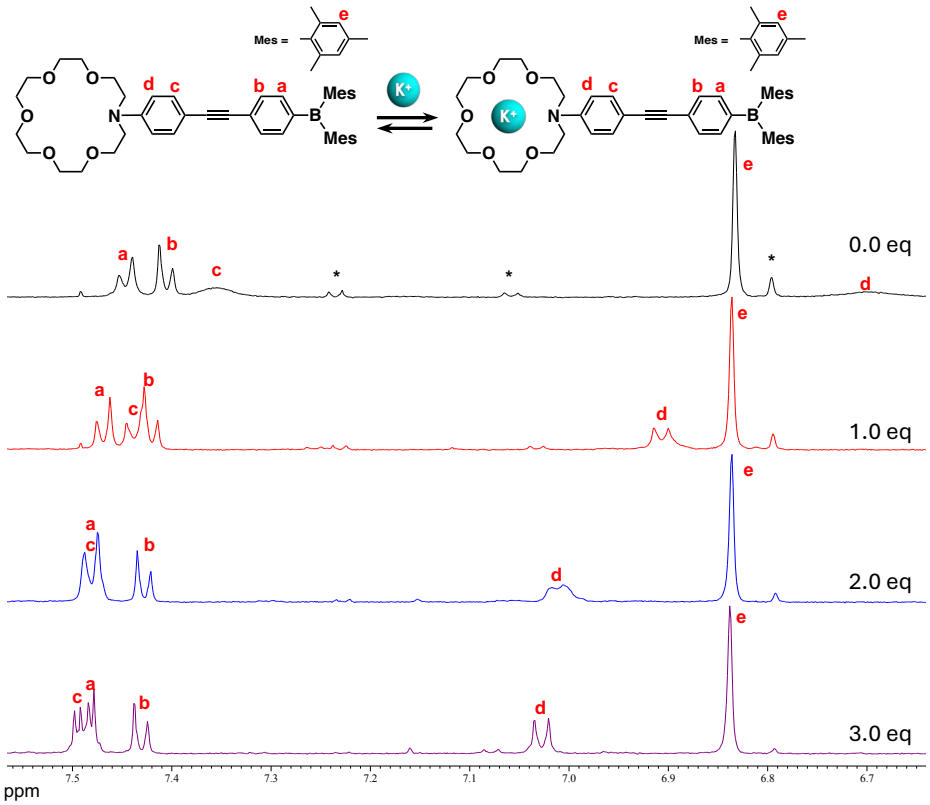

Fig. S22 ^{1}H NMR spectral changes of **L2** (1.2 mM) upon the addition of K^+ as PF_6^- salt in CD_2Cl_2/CD_3CN (1:1) at 25°C. * was not observed when only dichloromethane was used, and was therefore presumed to originate from the formation of a complex with acetonitrile.

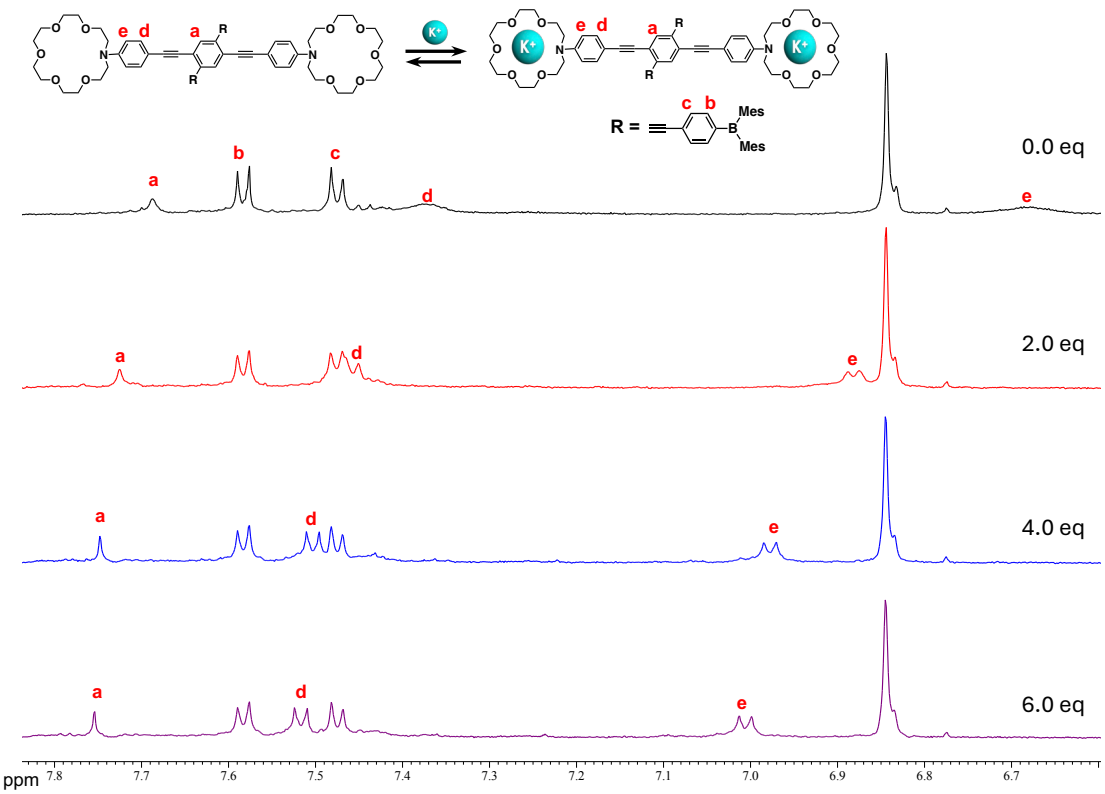

Fig. S23 ^{1}H NMR spectral changes of **X1** (0.6 mM) upon the addition of K^+ as PF_6^- salt in CD_2Cl_2/CD_3CN (1:1) at 25°C.

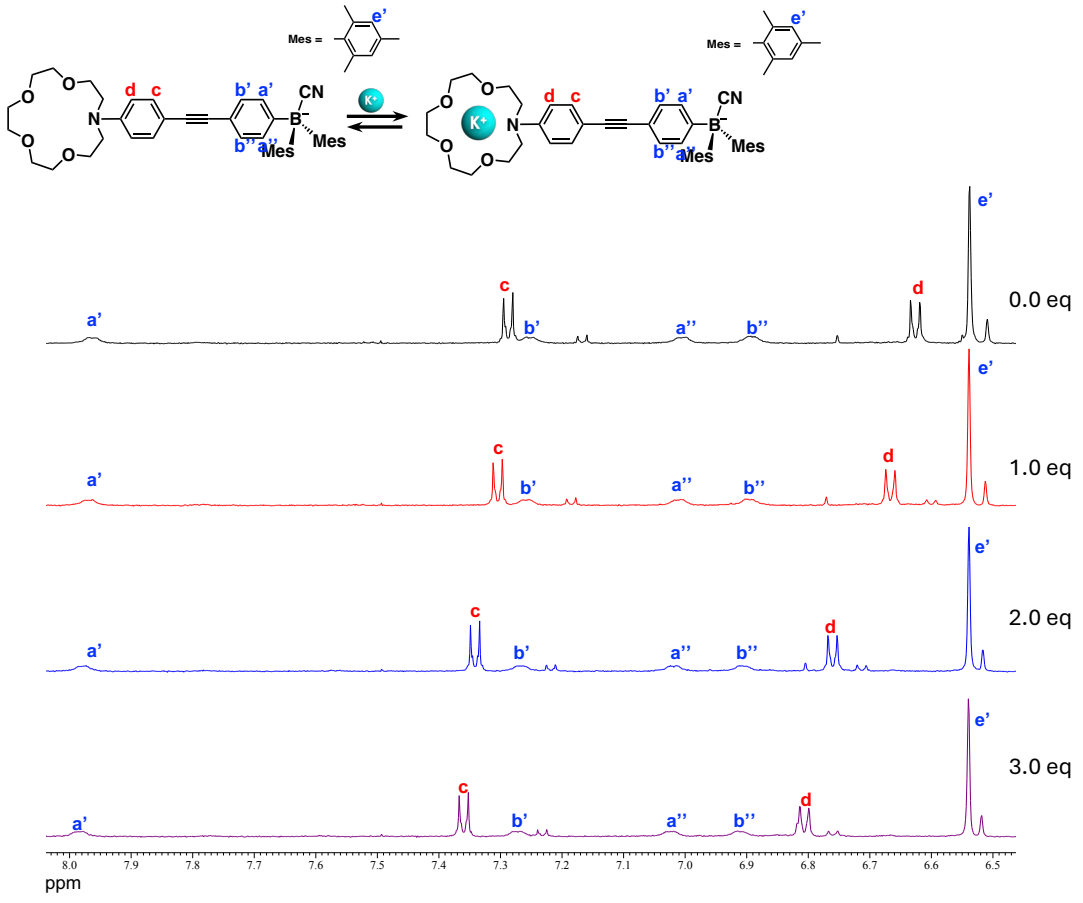

Fig. S24 ^{1}H NMR spectral changes of **L1**–CN (1.2 mM) upon the addition of K^+ as PF_6^- salt in CD_2Cl_2/CD_3CN (1:1) at 25°C. **L1**–CN was prepared by the mixture of **L1** and 3 eq. of TBACN.

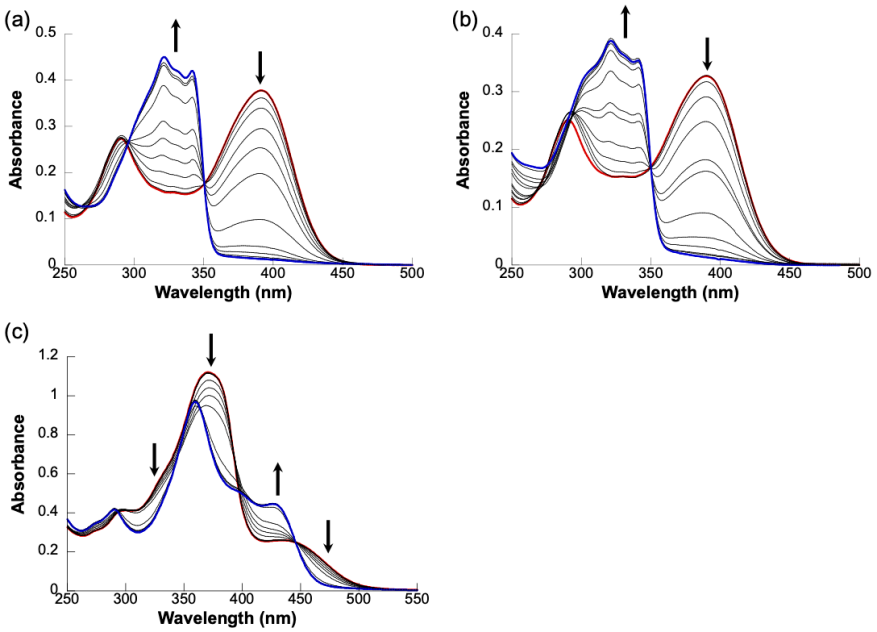

Fig. S25 UV/vis absorption spectral changes of (a) **L1**, (b) **L2**, and (c) **X1** upon the addition of F^- as TBA salt in CH_2Cl_2 (10^{-5} M).

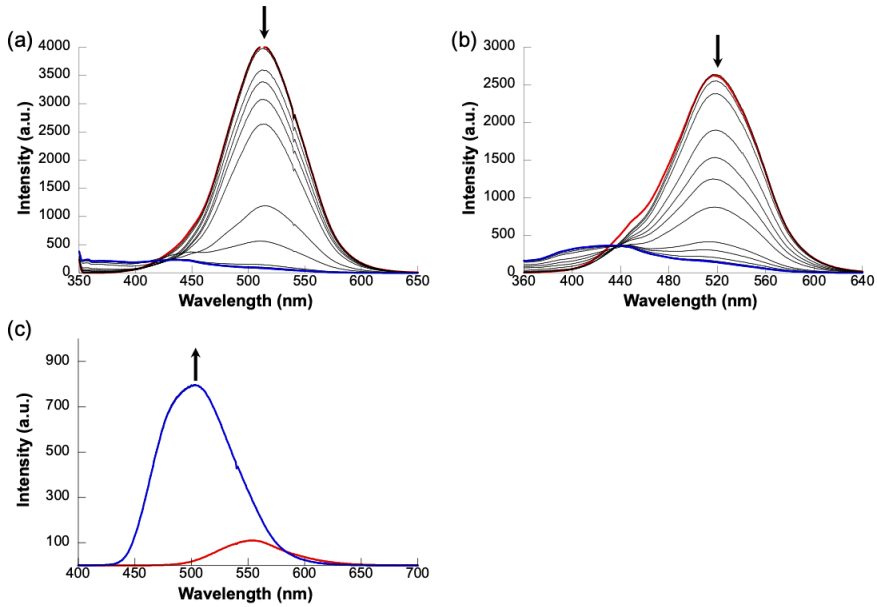

Fig. S26 Fluorescence spectral changes of (a) **L1**, (b) **L2**, and (c) **X1** upon the addition of F^- as TBA salt in CH_2Cl_2 (10^{-5} M). The fluorescence spectra of (a) and (b) were obtained by excitation at isosbestic points of anion titration, and (c) were obtained by excitation at absorption maxima. (See Fig. S25).

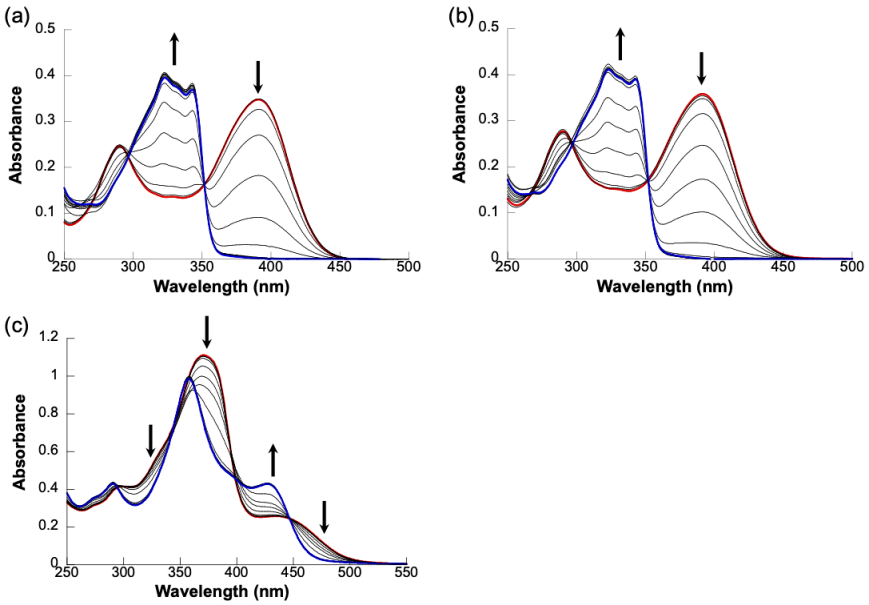

Fig. S27 UV/vis absorption spectral changes of (a) **L1**, (b) **L2**, and (c) **X1** upon the addition of CN^- as TBA salt in CH_2Cl_2 (10^{-5} M).

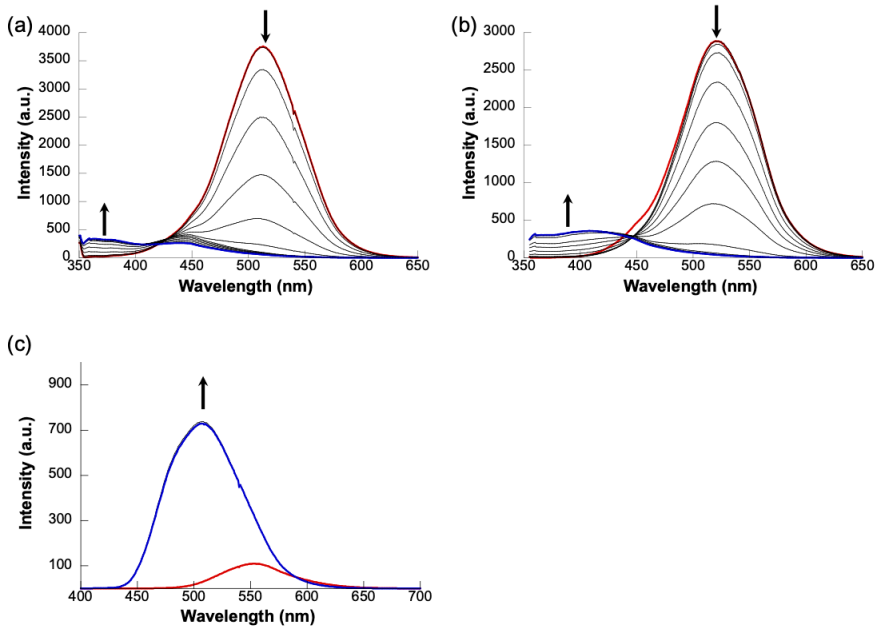

Fig. S28 Fluorescence spectral changes of (a) **L1**, (b) **L2**, and (c) **X1** upon the addition of CN^- as TBA salt in CH_2Cl_2 (10^{-5} M). The fluorescence spectra of (a) and (b) were obtained by excitation at isosbestic points of anion titration, and (c) were obtained by excitation at absorption maxima. (See Fig. S27).

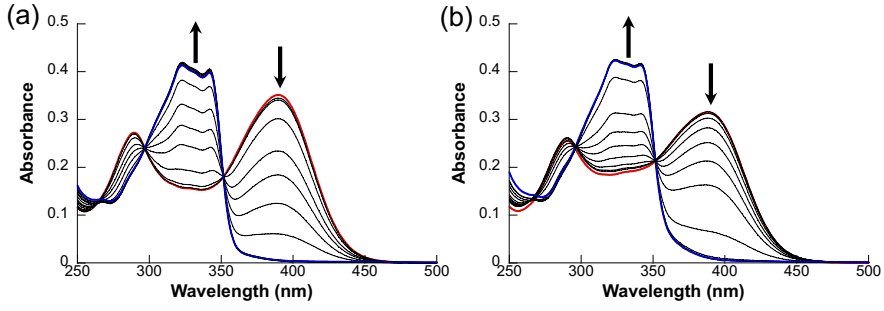

Fig. S29 UV/vis absorption spectral changes of (a) **L1** and (b) **L2** upon the addition of CN^- as TBA salt in CH_2Cl_2/MeCN (1:1) (10^{-5} M).

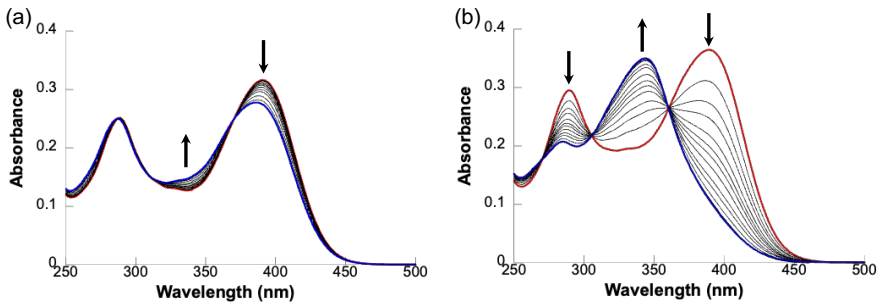

Fig. S30 UV/vis absorption spectral changes of (a) **L1** and (b) **L2** upon the addition of K^+ as PF_6 salt in CH_2Cl_2/MeCN (1:1) (10^{-5} M).

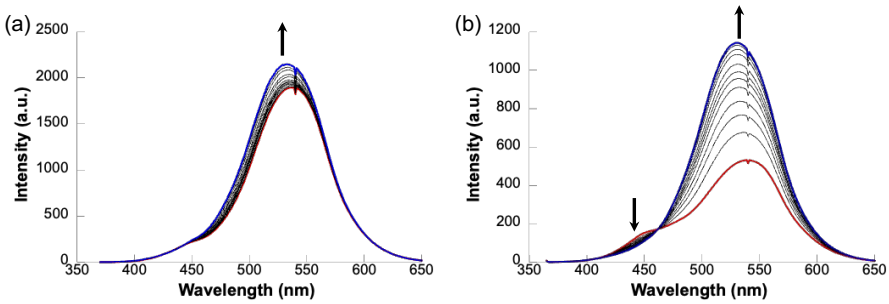

Fig. S31 Fluorescence spectral changes of (a) **L1** and (b) **L2** upon the addition of K^+ as PF_6 salt in CH_2Cl_2/MeCN (1:1) (10^{-5} M). The fluorescence spectra were obtained by excitation at isosbestic points of anion titration. (See Fig. S30).

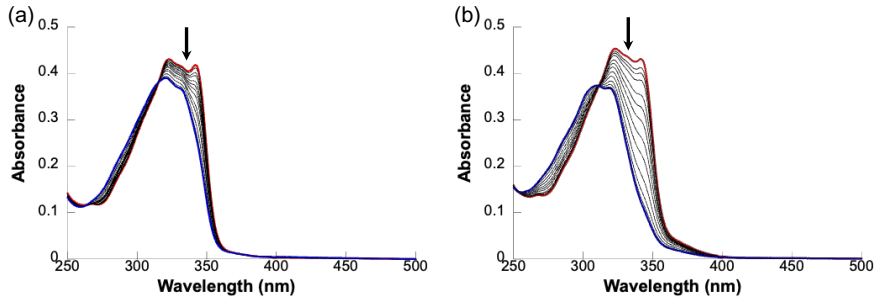

Fig. S32 UV/vis absorption spectral changes of (a) **L1**–CN and (b) **L2**–CN upon the addition of K^+ as KPF_6 salt in CH_2Cl_2/MeCN (1:1) (10^{-5} M). **L1**–CN and **L2**–CN were prepared by the mixture of **L1** and **L2** and 3 eq. of TBACN.

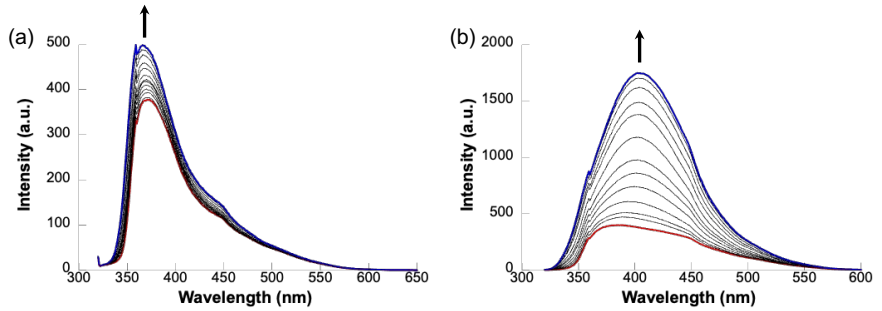

Fig. S33 Photoluminescence spectral changes of (a) **L1**–CN and (b) **L2**–CN upon the addition of K^+ as KPF_6 salt in CH_2Cl_2/MeCN (1:1) (10^{-5} M). **L1**–CN and **L2**–CN were prepared by the mixture of **L1** and **L2** with 3 eq. of TBACN. The fluorescence spectra were obtained by excitation at isosbestic points of anion titration. (See Fig. S32).

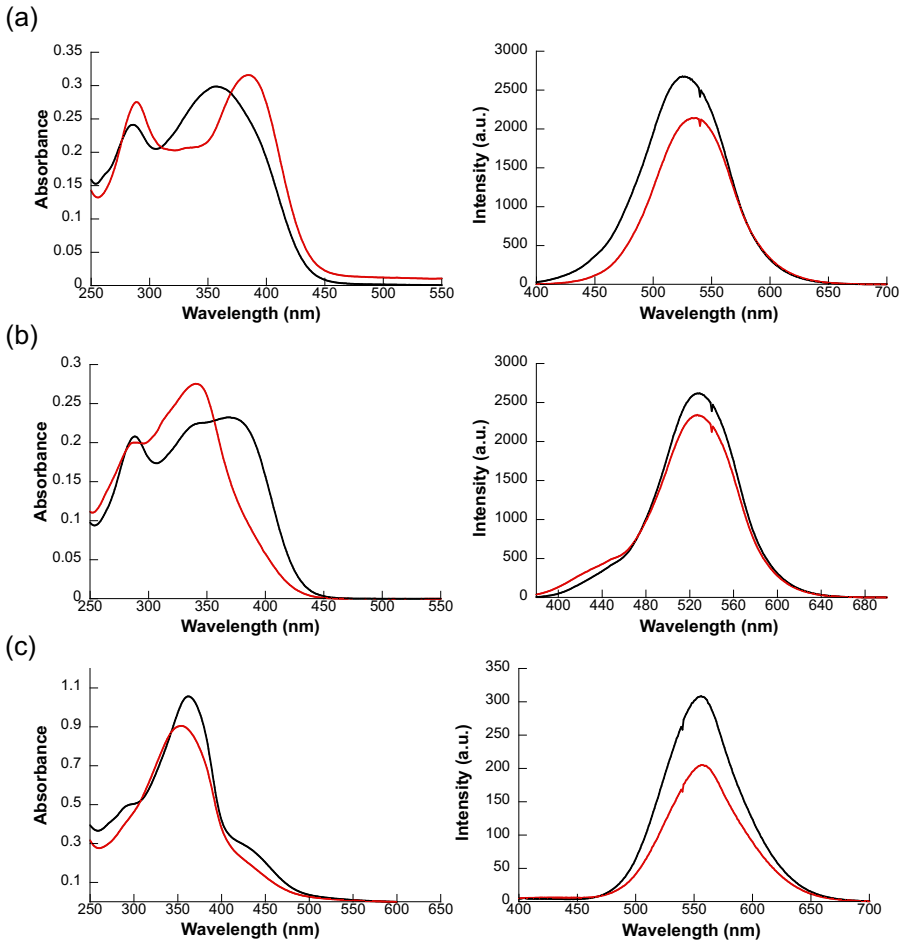

Fig. S34 UV/vis absorption (left) and fluorescence (right) spectra of (a) **L1**, (b) **L2**, and (c) **X1** upon addition of excess $NaClO_4$ (black) and KPF_6 (red) in CH_2Cl_2/MeCN (1:1). The fluorescence spectra were obtained by excitation at absorption maxima.

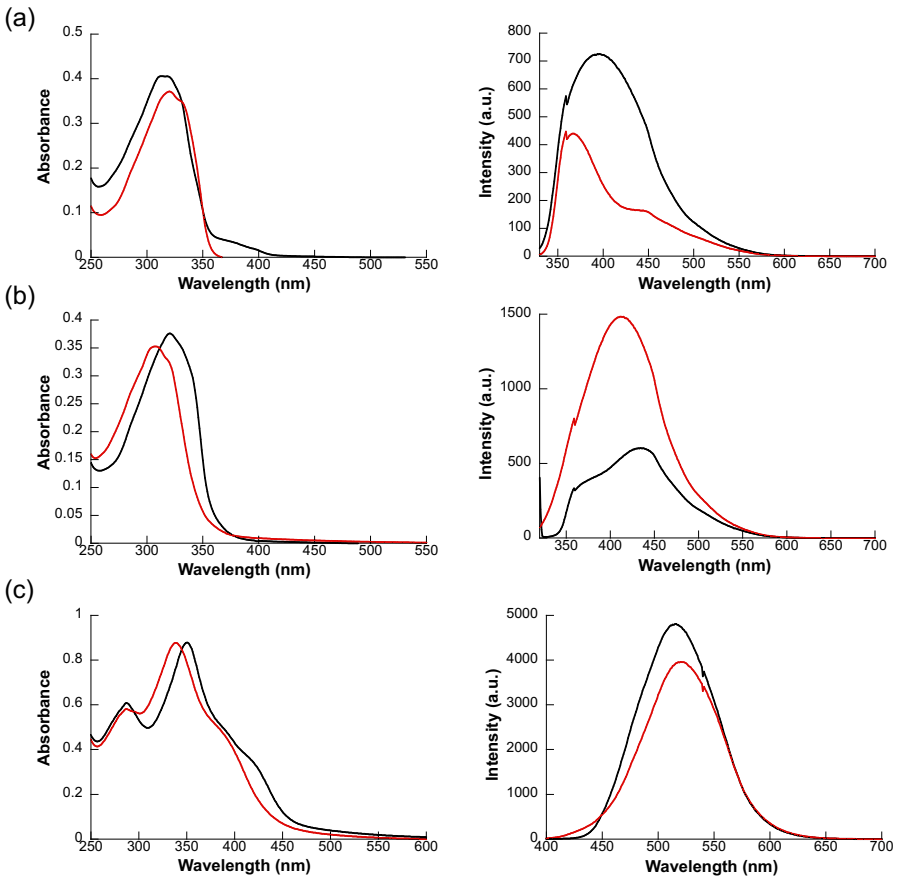

Fig. S35 UV/vis absorption (left) and fluorescence (right) spectra of (a) **L1**–CN, (b) **L2**–CN, and (c) **X1**–$(CN)_2$ upon addition of excess $NaClO_4$ (black) and KPF_6 (red) in CH_2Cl_2/MeCN (1:1). The fluorescence spectra were obtained by excitation at absorption maxima.

Table S1 Summary of fluorescence quantum yields (Φ_F) of **L1**, **L2**, and **X1** in CH_2Cl_2/MeCN (1:1).

	Φ_F (%)					
	free	+TBACN	+KPF_6	+$NaClO_4$	+TBACN/KPF_6	+TBACN/$NaClO_4$
L1	54	5	60	>99	7	13
L2	44	8	>99	87	31	10
X1	12	>99	26	28	>99	>99

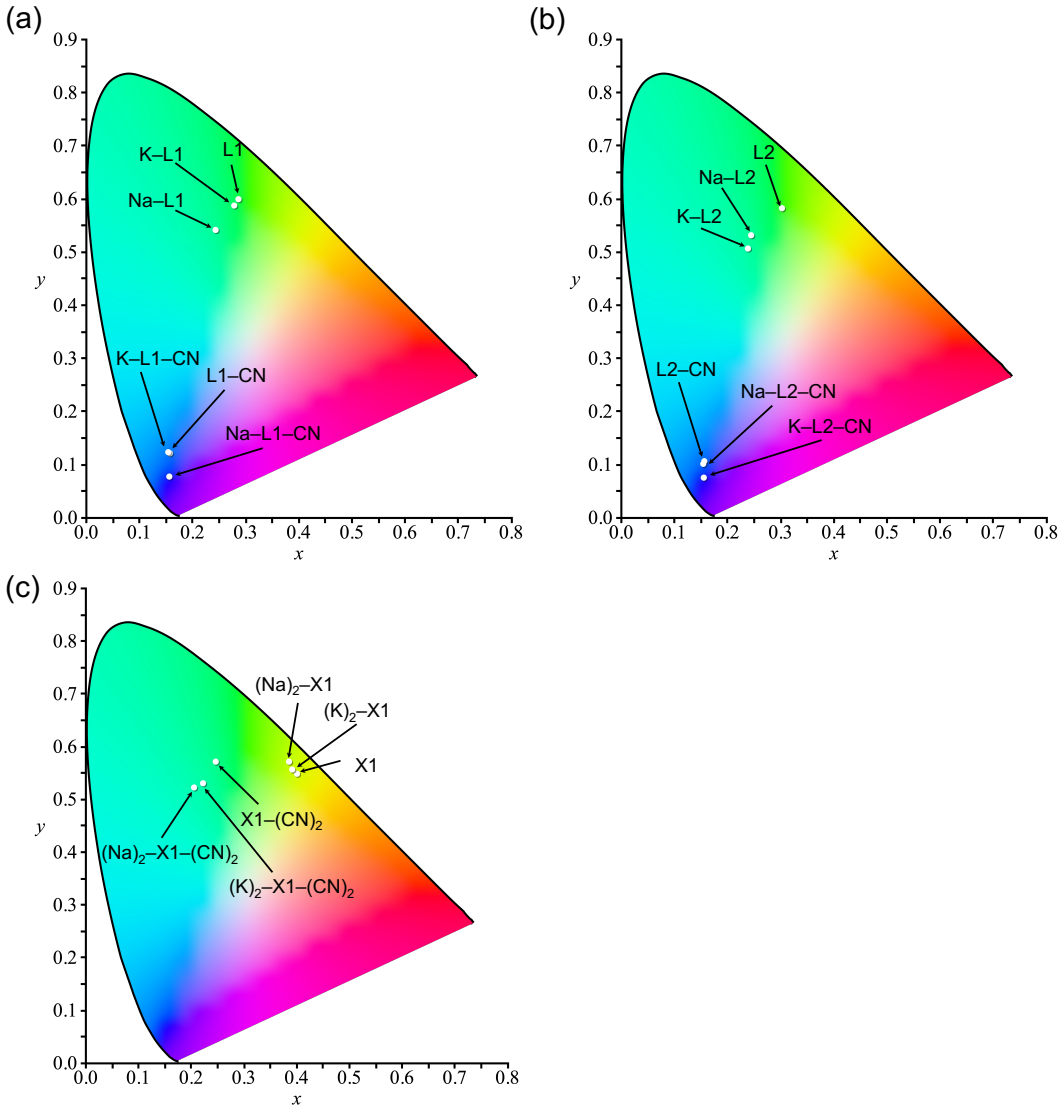

Fig. S36 Emission colour coordinates of (a) **L1**, (b) **L2**, and (c) **X1** with various ion pairs in the CIE 1931 chromaticity diagram.

Table S2 Summary of emission colour coordinates of **L1**, **L2**, and **X1** with various ion pairs in the CIE 1931 chromaticity diagram.

	L1	**L2**	**X1**
free	(0.286,0.601)	(0.302,0.584)	(0.400,0.550)
+TBACN	(0.157,0.122)	(0.156,0.107)	(0.246,0.573)
+KPF_6	(0.278,0.589)	(0.238,0.508)	(0.391,0.558)
+$NaClO_4$	(0.243,0.543)	(0.244,0.533)	(0.385,0.573)
+TBACN +KPF_6	(0.154,0.124)	(0.155,0.076)	(0.222,0.532)
+TBACN +$NaClO_4$	(0.156,0.078)	(0.154,0.102)	(0.205,0.524)

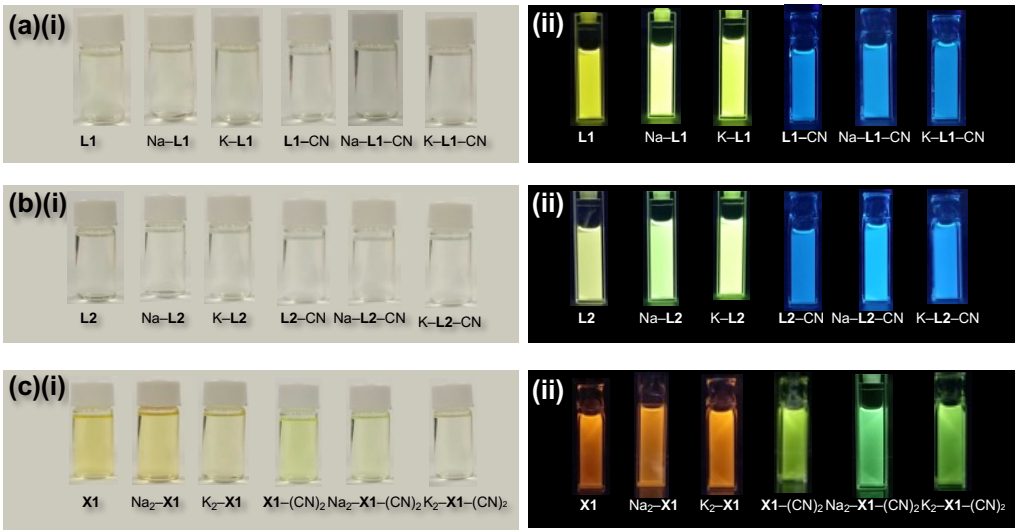

Fig. S37 Photographs of (a) **L1**, (b) **L2**, and (c) **X1** with various ion pairs (i) under visible light and (ii) UV irradiation.

4. Theoretical calculations

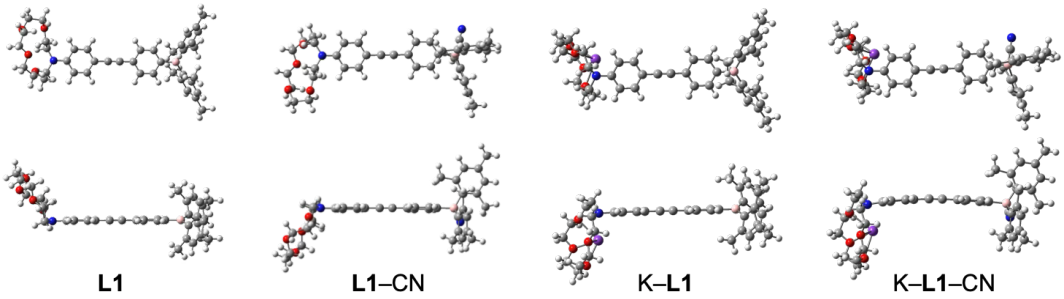

Fig. S38 Optimized structures of **L1**, **L1**–CN, K–**L1**, and K–**L1**–CN at B3LYP/6-31G(d,p) level.

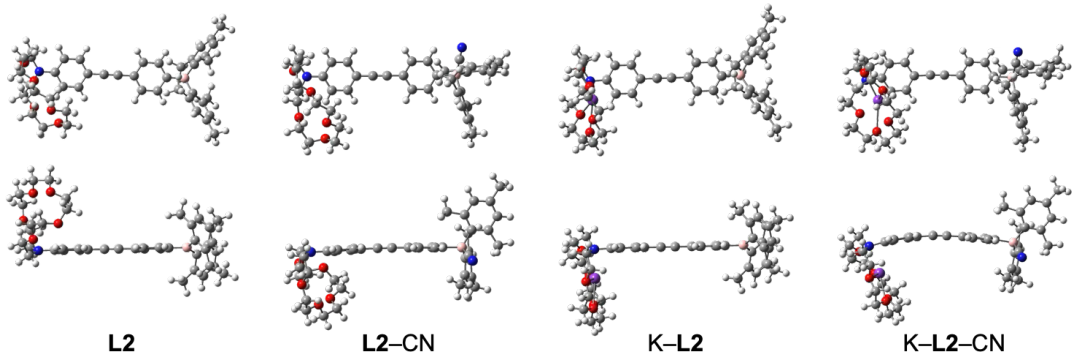

Fig. S39 Optimized structures of **L2**, **L2**–CN, K–**L2**, and K–**L2**–CN at B3LYP/6-31G(d,p) level.

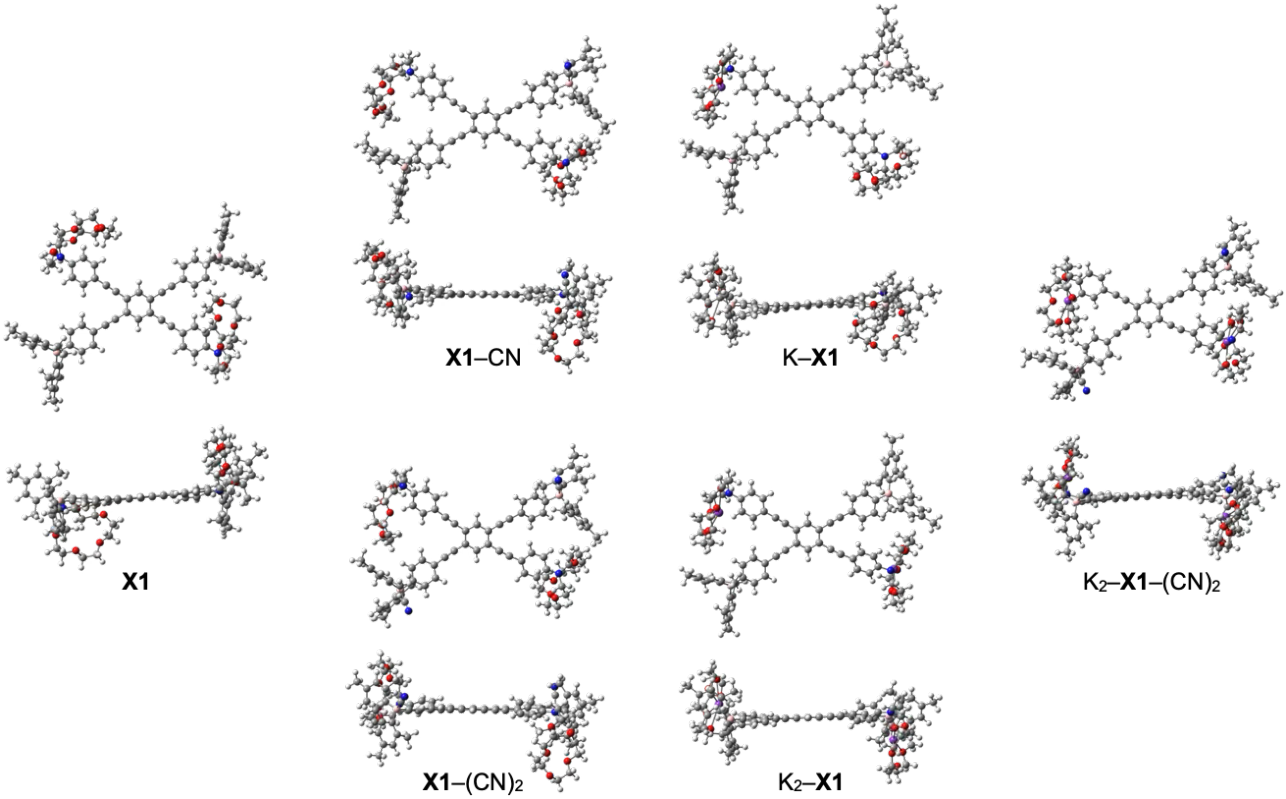

Fig. S40 Optimized structures of **X1**, **X1**–CN, **X1**–$(CN)_2$, K–**X1**, K_2–**X1** and K_2–**X1**–$(CN)_2$ at B3LYP/6-31G(d,p) level.

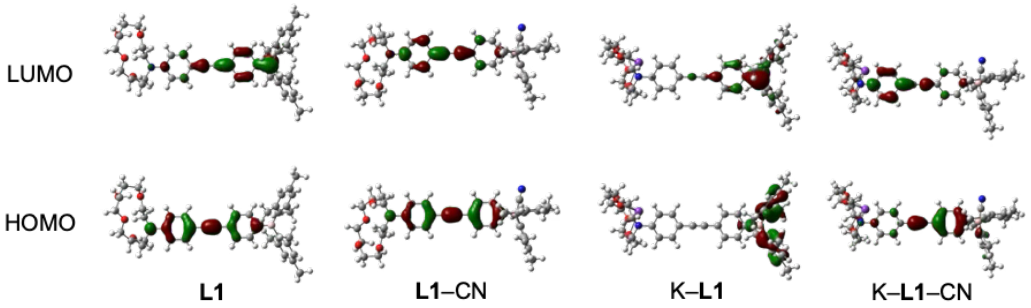

Fig. S41 Frontier molecular orbitals (HOMO and LUMO) of **L1**, **L1**–CN, K–**L1** and K–**L1**–CN calculated at TD-cam-B3LYP/6-31G(d)//B3LYP/6-31G(d,p) level. Although the HOMO and LUMO are localized predominantly on the donor and acceptor units, respectively, both orbitals are delocalized over the diphenylacetylene framework.

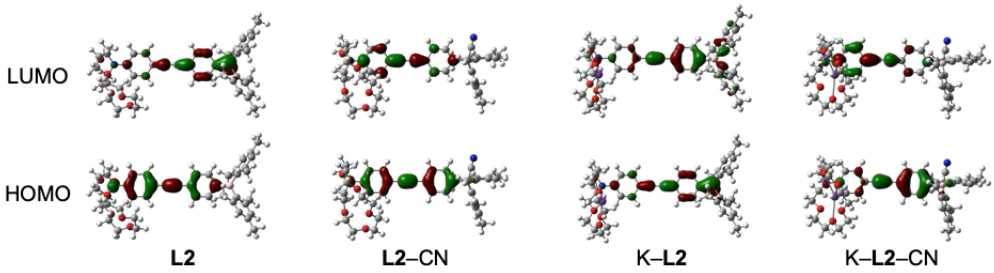

Fig. S42 Frontier molecular orbitals (HOMO and LUMO) of **L2**, **L2**–CN, K–**L2** and K–**L2**–CN calculated at TD-cam-B3LYP/6-31G(d)//B3LYP/6-31G(d,p) level. Although the HOMO and LUMO are localized predominantly on the donor and acceptor units, respectively, both orbitals are delocalized over the diphenylacetylene framework.

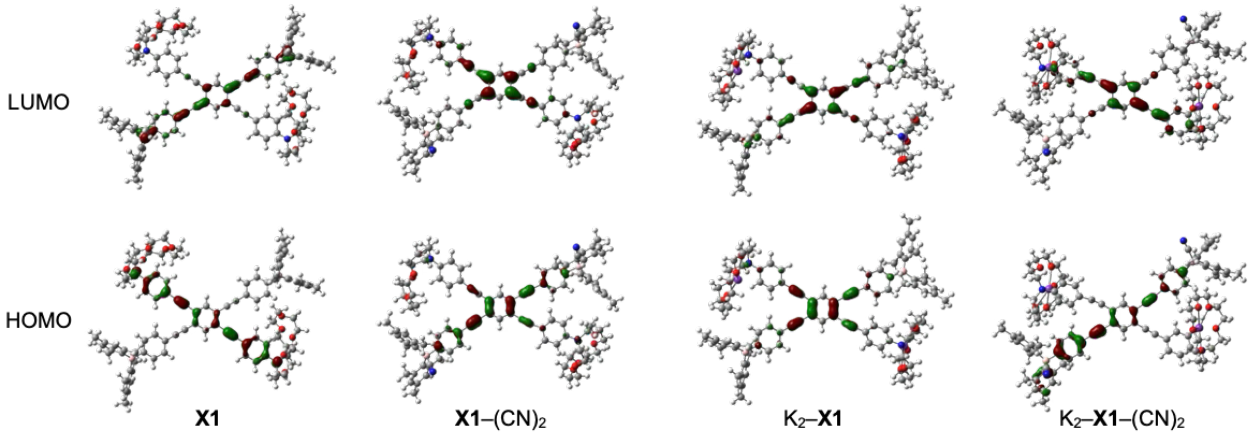

Fig. S43 Frontier molecular orbitals (HOMO and LUMO) of **X1**, **X1**–$(CN)_2$, K_2–**X1** and K_2–**X1**–$(CN)_2$ calculated at TD-cam-B3LYP/6-31G(d)//B3LYP/6-31G(d,p) level. In compound **X1**, the HOMO and LUMO are localized on the bis(phenylethynyl)benzene units bearing the azacrown ether and the dimesitylborane moieties, respectively. In contrast, in K_2– **X1**–$(CN)_2$, the HOMO is localized on the bis(phenylethynyl)benzene substituted with the boron–anion complex, while the LUMO is localized on the counterpart bearing the azacrown ether–cation complex. These results indicate that, even in the ion-pair complex, the HOMO and LUMO remain spatially separated, similar to the ion-free form.

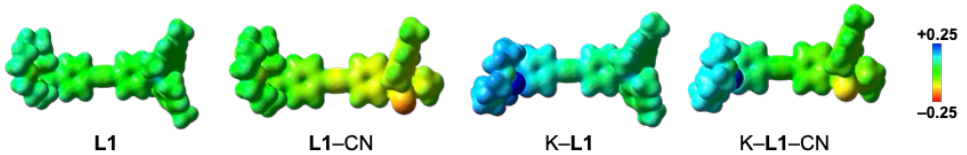

Fig. S44 Electron density diagrams of **L1**, **L1**–CN, K–**L1**, and K–**L1**–CN estimated by electrostatic potential (ESP) mapped onto the electron density isosurface (% = 0.01) calculated at B3LYP/6-31+G(d,p) level for the optimized structures.

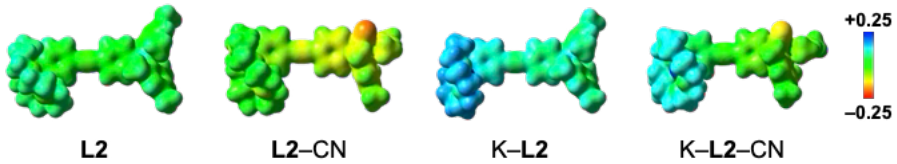

Fig. S45 Electron density diagrams of **L2**, **L2**–CN, K–**L2**, and K–**L2**–CN estimated by electrostatic potential (ESP) mapped onto the electron density isosurface (% = 0.01) calculated at B3LYP/6-31+G(d,p) level for the optimized structures.

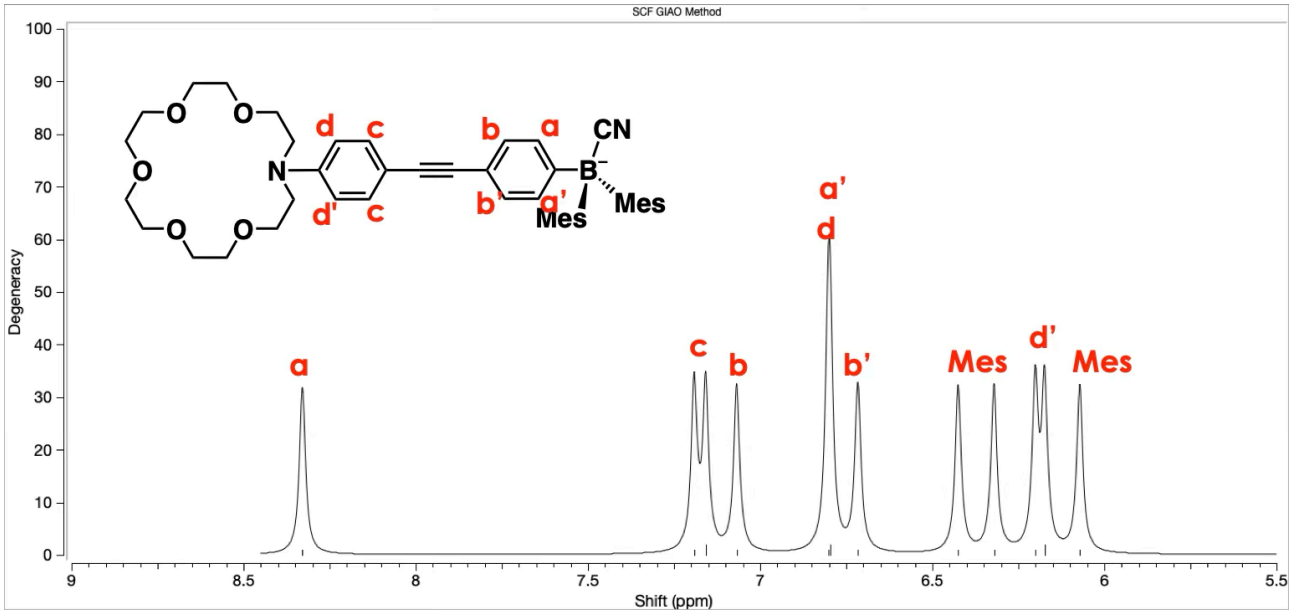

Fig. S46 Simulated ^{1}H NMR spectrum of **L2**–CN calculated at GIAO B3LYP/6-311+G(d)//B3LYP/6-31G(d,p).

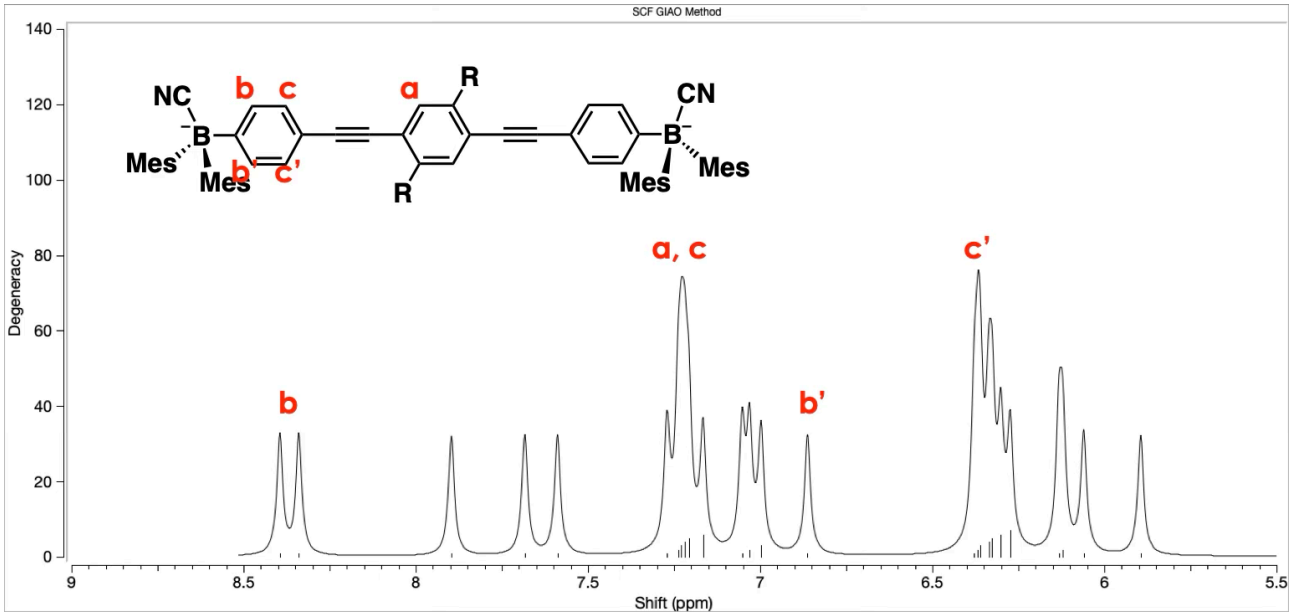

Fig. S47 Simulated ^{1}H NMR spectrum of **X1**–$(CN)_2$ calculated at GIAO B3LYP/6-311+G(d)//B3LYP/6-31G(d,p).